University of Amsterdam

Finite bond dimension scaling with the corner transfer matrix renormalization group method

supervisor: Dr. P. Corboz
second examiner: Prof. Dr. B. Nienhuis

Geert Kapteijns

Contents

1
Introduction

We investigate finite-size scaling behaviour in two-dimensional classical systems using the corner transfer matrix renormalization group (CTMRG) method. Instead of scaling in the system size N, we perform a scaling analysis in the bond dimension – or numbers of basis states kept – in approximating the corner transfer matrix of the system. This dimension is denoted m, though in other works it may appear as χ.

This thesis is laid out as follows. Chapter two introduces the density matrix renormalization group (DMRG) method in the context of one-dimensional quantum systems. Since most of the literature and research focuses on quantum lattice models, it is helpful to keep this picture in mind.

Chapter three explains how the ideas of DMRG can be applied to two-dimensional classical lattices. After making this connection clear, the corner transfer matrix renormalization group (CTMRG) method, a unification of DMRG and earlier ideas from Baxter, is introduced.

Chapter four introduces the concepts of critical behaviour and finite-size scaling, while chapter five makes the connection to finite-size effects that appear as a consequence of a finite bond dimension m within the CTMRG method.

Chapter six describes implementation details and convergence behaviour of the CTMRG algorithm. Chapter seven presents numerical results of finite-m scaling for the Ising model.

Chapter eight introduces the clock model and the basic concepts of the Kosterlitz-Thouless transition, presents results of finite-m scaling and compares with works using other numerical methods.

2

Density matrix renormalization group method

The density matrix renormalization group, proposed in 1992 by White [1], is introduced in its historical context. To highlight the ideas that led to this method, we explain the real-space renormalization group, proposed by Wilson [2] in 1975. We then explain how the shortcomings of Wilson's method led to the density matrix renormalization group.

2.1 Introduction

Consider the problem of numerically finding the ground state $|\Psi_0\rangle$ of an N-site one-dimensional spin-$\frac{1}{2}$ system.

The underlying Hilbert space of the system is a tensor product of the local Hilbert spaces $\mathscr{H}_{\text{site}}$, which are spanned by the states $\{|\uparrow\rangle, |\downarrow\rangle\}$. Thus, a general state of the system is a unit vector in a 2^N-dimensional space

$$|\Psi\rangle = \sum_{\sigma_1,\sigma_2,\ldots\in\{|\uparrow\rangle,|\downarrow\rangle\}} c_{\sigma_1,\sigma_2,\ldots,\sigma_N} |\sigma_1\rangle \otimes |\sigma_2\rangle \otimes \ldots \otimes |\sigma_N\rangle . \tag{2.1}$$

For a system with 1000 particles, the dimensionality of the Hilbert space comes in at about 10^{301}, some 220 orders of magnitude larger than the number of atoms in the observable universe. How can we possibly hope to approximate states in this space?

As it turns out, nature is very well described by Hamiltonians that are local – that do not contain interactions between an arbitrary number of bodies. And for these Hamiltonians, only an exponentially small subset of states can be explored in the lifetime of the universe [3]. That is, only exponentially few states are physical. The low-energy states, especially, have special properties that allow them to be very well approximated by a polynomial number

of parameters. This explains the existence of algorithms, of which the density matrix normalization group is the most widely celebrated one, that can approximate certain quantum systems to machine precision.

Refer to where this will be made more precise.

2.2 Density matrix renormalization group

The density matrix renormalization group (DMRG), introduced in 1992 by White [1], aims to find the best approximation of a many-body quantum state, given that only a fixed amount of basis vectors is kept. This amounts to finding the best truncation

$$\mathscr{H}_N \to \mathscr{H}_{\text{eff}} \tag{2.2}$$

from the full N-particle Hilbert space to an effective lower dimensional one. This corresponds to renormalizing the Hamiltonian H.

Before DMRG, several methods for achieving this truncation were proposed, most notably Wilson's real-space renormalization group [2]. We will discuss this method first, and highlight its shortcomings, which eventually led to the invention of the density-matrix renormalization group method by White.

2.2.1 Real-space renormalization group

Consider again the problem of finding the ground state of a many-body Hamiltonian H. A natural way of renormalizing H in real-space is by partitioning the lattice in blocks, and writing H as

$$H = H_A \otimes \ldots \otimes H_A \tag{2.3}$$

where H_A is the Hamiltonian of a block.

Make figures.

The real-space renormalization procedure now entails finding an effective Hamiltonian H'_A of the two-block Hamiltonian $H_{AA} = H_A \otimes H_A$. In the method introduced by Wilson, H'_A is formed by keeping the m lowest lying eigenstates $|\epsilon_i\rangle$ of H_{AA}:

$$H'_A = \sum_{i=1}^{m} \epsilon_i \, |\epsilon_i\rangle \langle\epsilon_i| \, . \tag{2.4}$$

This is equivalent to writing

$$H'_A = OH_{AA}O^\dagger, \tag{2.5}$$

with O an $m \times 2^L$ matrix, with rows being the m lowest-lying eigenvectors of H_{AA}, and L the number of lattice sites of a block. At the fixed point of this iteration procedure, H_A represents the Hamiltonian of an infinite chain. In choosing this truncation, it is assumed that the low-lying eigenstates of the system in the thermodynamic limit are composed of low-lying eigenstates of smaller blocks.

It turns out that this method gives poor results for many lattice systems. Following an example put forth by White and Noack [4], we establish an intuition why.

2.2.2 Single particle in a box

Consider the Hamiltonian

$$H = 2\sum_i |i\rangle\langle i| - \sum_{\langle i,j\rangle} |i\rangle\langle j|, \tag{2.6}$$

where the second summation is over nearest neighbors $\langle i, j\rangle$. H represents the discretized version of the particle-in-a-box Hamiltonian, so we expect its ground state to be approximately a standing wave with wavelength double the box size. However, the blocking procedure just described tries to build the ground state iteratively from ground states of smaller blocks. No matter the amount of states kept, the final result will always incur large errors.

For this simple model, White and Noack solved the problem by diagonalizing the Hamiltonian of a block with different boundary conditions, and combining the lowest eigenstates of each.

Additionally, they noted that diagonalizing $p > 2$ blocks, and projecting out $p - 2$ blocks to arrive at H_{AA} also gives accurate results, and that this is a generalization of applying multiple boundary conditions.

Figure.

In the limit $p \to \infty$ this method becomes exact, since we then find exactly the correct contribution of H_{AA} to the final ground state. It is a slightly changed version of this last method that is now known as DMRG.

2.2.3 Density matrix method

The fundamental idea of the density matrix renormalization group method rests on the fact that if we know the state of the final lattice, we can find the m most important states for H_{AA} by diagonalizing the reduced density matrix ρ_{AA} of the two blocks.

To see this, suppose, for simplicity, that the entire lattice is in a pure state[1] $|\Psi\rangle = \sum c_{b,e} |b\rangle |e\rangle$, with $b = 1, \ldots, l$ the states of H_{AA} and $e = 1, \ldots, N_{\text{env}}$ the environment states. The reduced density matrix is given by

$$\rho_{AA} = \sum_e |\Psi\rangle \langle\Psi| = \sum_{b,b'} c_{b,e} c_{b',e} |b\rangle \langle b'| \tag{2.7}$$

We now wish to find a set of orthonormal states $|\lambda\rangle \in \mathcal{H}_{AA}$, $\lambda = 1, \ldots, m$ with $m < l$, such that the quadratic norm

$$\| |\Psi\rangle - |\widetilde{\Psi}\rangle \| = 1 - 2 \sum_{\lambda,b,e} a_{\lambda,e} c_{b,e} u_{\lambda,b} + \sum_{\lambda,e} a_{\lambda,e}^2 \tag{2.8}$$

is minimized. Here,

$$|\widetilde{\Psi}\rangle = \sum_{\lambda=1}^{m} \sum_{e=1}^{N_{\text{env}}} a_{\lambda,e} |\lambda\rangle |e\rangle \tag{2.9}$$

is the representation of $|\Psi\rangle$ given the constraint that we can only use m states from $\mathcal{H}_{AA}$. The $u_{\lambda,b}$ are given by

$$\lambda = \sum_b u_{\lambda,b} |b\rangle . \tag{2.10}$$

We need to minimize (2.8) with respect to $a_{\lambda,e}$ and $u_{\lambda,b}$. Setting the derivative with respect to $a_{\lambda,e}$ equal to 0 yields

$$-2 \sum_{\lambda,b,e} c_{b,e} u_{\lambda,b} + 2 \sum_{\lambda,e} a_{\lambda,e} = 0 \tag{2.11}$$

So we see that $a_{\lambda,e} = \sum_b c_{b,e} u_{\lambda,b}$, and we are left to minimize

$$1 - \sum_{\lambda,b,b'} u_{\lambda,b} (\rho_{AA})_{b,b'} u_{\lambda,b'} \tag{2.12}$$

[1] For a proof for a mixed state, see [5]

with respect to $u_{\lambda,b}$. But this is equal to

$$1 - \sum_{\lambda=1}^{m} \langle \lambda | \, \rho_{AA} \, | \lambda \rangle \tag{2.13}$$

and because the eigenvalues of ρ_{AA} represent probabilities and are thus non-negative, this is clearly minimal when $|\lambda\rangle$ are the m eigenvectors of ρ_{AA} corresponding to the largest eigenvalues. This minimal value is

$$1 - \sum_{\lambda=1}^{m} w_\lambda \tag{2.14}$$

with w_λ the eigenvalues of the reduced density matrix.

Eq. 2.14 is called the truncation error or residual probability, and quantifies the incurred error when taking a number $m < l$ states to represent $\mathcal{H}_{AA}$.

We have proven that the optimal (in the sense that $\| \, |\Psi\rangle - |\widetilde{\Psi}\rangle \, \|$ is minimized[2]) states to keep for a subsystem are the states given by the reduced density matrix, obtained by tracing out the entire lattice in the ground state (or some other target state).

The problem, of course, is that we do not know the state of the entire lattice, since that is exactly what we're trying to approximate.

Instead then, we should try to calculate the reduced density matrix of the system embedded in *some* larger environment, as closely as possible resembling the one in which it should be embedded. The combination of the system block and this environment block is usually called *superblock*.

Analogous to how White and Noack solved the particle in a box problem, we could calculate the ground state of $p > 2$ blocks, and trace out all but 2, doubling our block size each iteration. In practice, this doesn't work well for interacting Hamiltonians, since this would involve finding the largest eigenvalue of a $N_{\text{block}}^{p} \times N_{\text{block}}^{p}$ matrix (compare this with the particle in a box Hamiltonian, which only grows linearly in the amount of lattice sites).

The widely adopted algorithm proposed by White [7] for finding the ground state of a system in the thermodynamic limit proceeds as follows.

[2] There are several other arguments for why these states are optimal, for example, they minimize the error in expectation values $\langle A \rangle$ of operators. For an overview, see [6].

2.2.4 Infinite-system method

Add figures.

Mention boundary conditions somewere

Instead of using an exponential blocking procedure (doubling or tripling the amount of effective sites in a block at each iteration), the infinite-system method in the DMRG formulation adds a single site before truncating the Hilbert space to have at most m basis states.

1. Consider a block A of size l, with l small. Suppose, for simplicity, that the number of basis states of the block is already m. States of this block can be written as
$$|\Psi_A\rangle = \sum_{b=1}^{m} c_i \, |b\rangle \, . \tag{2.15}$$
The Hamiltonian is written as (similarly for other operators):
$$\hat{H}_A = \sum_{b,b'}^{m} H_{bb'} \, |b\rangle \, \langle b| \, . \tag{2.16}$$

2. Construct an enlarged block with one additional site, denoted by $A\cdot$. States are now written
$$|\Psi_{A\cdot}\rangle = \sum_{b,\sigma} c_{b,\sigma} \, |b\rangle \otimes |\sigma\rangle \, . \tag{2.17}$$
Here, σ runs over the d local basis states of $\mathscr{H}_{\text{site}}$.

3. Construct a superblock, consisting of the enlarged system block $A\cdot$ and a reflected environment block $\cdot A$, together denoted by $A\cdot\cdot A$. Find the ground state $|\Psi_0\rangle$ of $A\cdot\cdot A$, for example with the Lanczos method [8].

4. Obtain the reduced density matrix of the enlarged block by tracing out the environment, and write it in diagonal form.
$$\begin{aligned} \rho_{A\cdot} &= \sum_{e,\sigma} (\langle\sigma| \otimes \langle e|) \, |\Psi_0\rangle \, \langle\Psi_0| \, (|\sigma\rangle \otimes |e\rangle), \\ &= \sum_{i=1}^{dm} w_i \, |\lambda_i\rangle \, \langle\lambda_i| \, . \end{aligned} \tag{2.18}$$

Here, we have chosen $w_0 >= w_1 \ldots >= w_{dm}$. In this basis, the Hamiltonian is written as

$$\hat{H}_{A\cdot} = \sum_{i,j}^{dm} H_{ij} \left|\lambda_i\right\rangle \left\langle\lambda_j\right| . \tag{2.19}$$

5. Truncate the Hilbert space by keeping only the m eigenstates of $\rho_{A\cdot}$ with largest eigenvalues. Operators truncate as follows:

$$\widetilde{\rho}_{A\cdot} = \sum_{i=1}^{m} w_i \left|\lambda_i\right\rangle \left\langle\lambda_j\right| , \tag{2.20}$$

$$\widetilde{H}_{A\cdot} = \sum_{i,j}^{m} H_{ij} \left|\lambda_i\right\rangle \left\langle\lambda_j\right| . \tag{2.21}$$

6. Set $H_A \leftarrow \widetilde{H}_{A\cdot}$ and return to 1.

Expand. Present or link to some results. Finite-system algorithm. Maybe in other chapter: rephrase in MPS, validity of approximation: primer on entropy and eigenvalue spectrum of density matrix.

This methods finds ground state energies with astounding accuracy, and has been the reference point in all 1D quantum lattice simulation since its invention.

3

DRMG applied to two-dimensional classical lattice models

This chapter explains how to apply to ideas of the density matrix renormalization group to two-dimensional classical lattices.

First, we explain the transfer-matrix formulation for classical partition functions.

Then, we show how to renormalize the transfer matrix using DMRG. This was first done by Nishino [9]. To make notation easier and up-to-date with current approaches, we redefine the transfer matrix in terms of a tensor network.

Then, we explain the corner transfer matrix renormalization group (CTMRG) method. This method, first introduced by Nishino and Okunishi [10], unifies ideas from Baxter [11–13] and White [1] to significantly speed up the renormalization of the transfer matrix.

3.1 Statistical mechanics on classical lattices

For a general introduction to statistical mechanics, we refer to [14].

The central quantity in equilibrium statistical mechanics is the partition function Z, which, for a discrete system such as a lattice, is defined as

$$Z = \sum_s \exp\left(-\beta H(s)\right), \tag{3.1}$$

where the sum is over all microstates s, H is the energy function, and $\beta = T^{-1}$ the inverse temperature.

The probability that the system is in a particular microstate

$$p(s) = \frac{\exp(-\beta H(s))}{Z} \tag{3.2}$$

is also called the *Boltzmann weight*.

At first glance, the partition function is a simple normalization factor. But its importance stems from the fact that since it contains all statistical information about the system, all thermodynamic quantities can be expressed as a function of Z.

The energy of the system is expressed as

$$\langle E \rangle = \frac{\sum_s H(s) \exp\left(-\beta H(s)\right)}{Z} = -\frac{\partial}{\partial \beta} \log Z, \tag{3.3}$$

the entropy as

$$S = -\sum_s p(s) \log p(s) = \frac{\partial}{\partial T}(T \log Z), \tag{3.4}$$

and the free energy as

$$F = \langle E \rangle - TS = T^2 \frac{\partial}{\partial T} \log Z - T \frac{\partial}{\partial T}(T \log Z) = -T \log Z. \tag{3.5}$$

3.2 Transfer matrices of lattice models

Transfer matrices are used to re-express the partition function of classical lattice systems, allowing them to be solved exactly or approximated.

We will introduce the transfer matrix in the context of the 1D classical Ising model, first introduced and solved using the transfer matrix method by Ising [15] in his PhD thesis.

3.2.1 1D Ising model

Consider the 1D ferromagnetic Ising model [15], defined by the energy function

$$H(\sigma) = -J \sum_{\langle ij \rangle} \sigma_i \sigma_j - h \sum_i \sigma_i. \tag{3.6}$$

Here, we sum over nearest neighbors $\langle ij \rangle$ and the spins σ_i take the values ± 1. $J > 0$ is the spin coupling and $h > 0$ an external magnetic field.

Assume, for the moment, that the chain consists of N spins, and apply periodic boundary conditions. The partition function of this system is given by

$$Z_N = \sum_{\sigma_1, \ldots, \sigma_N \in \{-1, 1\}} \exp(-\beta H(\sigma)) \tag{3.7}$$

Exploiting the local nature of the interaction between spins, we can write

$$Z_N = \sum_{\sigma_1,\cdots,\sigma_N \in \{-1,1\}} \prod_{\langle i,j \rangle} e^{K\sigma_i\sigma_j + \frac{H}{2}(\sigma_i+\sigma_j)} \tag{3.8}$$

where we defined $K \equiv \beta J$ and $H \equiv \beta h$.

Now, we define the 2×2 matrix

$$T_{\sigma\sigma'} = \exp(K\sigma\sigma' + \frac{H}{2}(\sigma + \sigma')). \tag{3.9}$$

for which a possible choice of basis is

$$(|\uparrow\rangle = 1, |\downarrow\rangle = -1) = (\begin{bmatrix}1\\0\end{bmatrix}, \begin{bmatrix}0\\1\end{bmatrix}). \tag{3.10}$$

In terms of this matrix, Z_N is written as

$$Z_N = \sum_{\sigma_1,\cdots,\sigma_N} T_{\sigma_1\sigma_2}\cdots T_{\sigma_N\sigma_1} = \mathrm{Tr}\, T^N. \tag{3.11}$$

T is called the transfer matrix. In the basis of Eq. 3.10, it is written as

$$T = \begin{bmatrix} e^{K+H} & e^{-K} \\ e^{-K} & e^{K-H} \end{bmatrix}. \tag{3.12}$$

T is, in fact, diagonalizable. So, we can write $T^N = PD^NP^{-1}$, where P consists of the eigenvectors of T, and D has the corresponding eigenvalues on the diagonal. By the cyclic property of the trace, we have

$$Z_N = \lambda_+^N + \lambda_-^N, \tag{3.13}$$

where

$$\lambda_\pm = e^K \left[\cosh(H) \pm \sqrt{\sinh^2(H) + e^{-4K}}\right] \tag{3.14}$$

Thus, we have reduced the problem of finding the partition function to an eigenvalue problem.

In the thermodynamic limit $N \to \infty$

$$Z = \lim_{N\to\infty} \lambda_+^N \tag{3.15}$$

where λ_+ is the non-degenerate largest eigenvalue (in absolute value) of T. Thermodynamic quantities like the free energy per site

$$\frac{F}{N} = -T \log \lambda_+ \tag{3.16}$$

and the magnetization per site

$$M = \frac{\sum_i^N \langle \sigma_i \rangle}{N} = -\frac{1}{N}\frac{\partial F}{\partial h} \tag{3.17}$$

can now readily be calculated.

3.2.1.1 Fixed boundary conditions

We may also apply fixed boundary conditions. The partition function is then written as

$$Z_N = \langle \sigma' | \, T^N \, | \sigma \rangle \,, \tag{3.18}$$

where $|\sigma\rangle$ and $|\sigma'\rangle$ are the right and left boundary spins.

In the large-N limit, T^N tends towards the projector onto the eigenspace spanned by the eigenvector belonging to the largest eigenvalue

$$|\lambda_+\rangle = \lim_{N\to\infty} \frac{T^N \, |\sigma\rangle}{\left\| T^N \, |\sigma\rangle \right\|}. \tag{3.19}$$

Eq. 3.19 is true for any $|\sigma\rangle$ that is not orthogonal to $|\lambda_+\rangle$.

The physical significance of the normalized lowest-lying eigenvector $|\lambda_1\rangle$ is that $\langle \lambda_1 | \uparrow \rangle$ and $\langle \lambda_1 | \downarrow \rangle$ represent the Boltzmann weight of $|\uparrow\rangle$ and $|\downarrow\rangle$ at the boundary of a half-infinite chain.

Maybe picture of above claim?

3.2.2 2D Ising model

Talk about exact solution (Onsager). Why is it important? Maybe star-triangle relation (Baxter). Not all IRF models solvable.

Next, we treat the two-dimensional, square-lattice Ising model. In two dimensions, the energy function is still written as in Eq. 3.6, but now every lattice site has four neighbors.

Let N be the number of columns and l be the number of rows of the lattice, and assume $l \gg N$. In the vertical direction, we apply periodic boundary conditions, as in the one-dimensional case. In the horizontal direction, we keep an open boundary. We refer to N as the system size.

Picture?

Similarly as in the 1D case, the partition function can be written as

$$Z_N = \sum_{\boldsymbol{\sigma}} \prod_{\langle i,j,k,l \rangle} W(\sigma_i, \sigma_j, \sigma_k, \sigma_l) \tag{3.20}$$

where the product runs over all groups of four spins sharing the same face. The Boltzmann weight of such a face is given by

$$W(\sigma_i, \sigma_j, \sigma_k, \sigma_l) = \exp\left\{\frac{K}{2}(\sigma_i\sigma_j + \sigma_j\sigma_k + \sigma_k\sigma_l + \sigma_l\sigma_i)\right\} \tag{3.21}$$

We can express the Boltzmann weight of a configuration of the whole lattice as a product of the Boltzmann weights of the rows

$$Z_N = \sum_{\boldsymbol{\sigma}} \prod_{r=1}^{l} W(\sigma_1^r, \sigma_2^r, \sigma_1^{r+1}, \sigma_2^{r+1}) \ldots W(\sigma_{N-1}^r, \sigma_N^r, \sigma_{N-1}^{r+1}, \sigma_N^{r+1}) \tag{3.22}$$

where σ_i^r denotes the value of the ith spin of row r.

Now, we can generalize the definition of the transfer matrix to two dimensions, by defining it as the Boltzmann weight of an entire row

$$T_N(\boldsymbol{\sigma}, \boldsymbol{\sigma'}) = W(\sigma_1, \sigma_2, \sigma_1', \sigma_2') \ldots W(\sigma_{N-1}, \sigma_N, \sigma_{N-1}', \sigma_N') \tag{3.23}$$

If we take the spin configurations of an entire row as basis vectors, T_N can be written as a matrix of dimensions $2^N \times 2^N$.

Similarly as in the one-dimensional case, the partition function now becomes

$$Z_N = \sum_{\boldsymbol{\sigma}} \prod_{r=1}^{l} T_N(\boldsymbol{\sigma}^r, \boldsymbol{\sigma}^{r+1}) = \operatorname{Tr} T_N^l \tag{3.24}$$

In the limit of an $N \times \infty$ cylinder, the partition function is once again determined by the largest eigenvalue[1].

$$Z_N = \lim_{l\to\infty} T_N^l = \lim_{l\to\infty} (\lambda_0)_N^l \tag{3.25}$$

[1] As in the 1D case, T is symmetric, so it is orthogonally diagonalizable.

The partition function in the thermodynamic limit is given by

$$Z = \lim_{N \to \infty} Z_N \tag{3.26}$$

3.3 Partition function of the 2D Ising model as a tensor network

In calculating the partition function of 1D and 2D lattices, matrices of Boltzmann weights like W and T play a crucial role. We have formulated them in a way that is valid for any interaction-round-a-face (IRF) model, defined by

$$H \propto \sum_{\langle i,j,k,l \rangle} W(\sigma_i, \sigma_j, \sigma_k, \sigma_l), \tag{3.27}$$

where the summation is over all spins sharing a face. W can contain 4-spin, 3-spin, 2-spin and 1-spin interaction terms. The Ising model is a special case of the IRF model, with W given by Eq. 3.21.

We will now express the partition function of the 2D Ising model as a tensor network. The transfer matrix T is redefined in the process. This allows us to visualize the equations in a way that is consistent with the many other tensor network algorithms under research today. For an introduction to tensor network notation, see Appendix B.

3.3.1 Tensor network of the partition function of a system of four spins

We define

$$Q(\sigma_i, \sigma_j) = \exp(K \sigma_i \sigma_j) \tag{3.28}$$

as the Boltzmann weight of the bond between σ_i and σ_j. It is the same as the 1D transfer matrix in Eq. 3.9.

The Boltzmann weight of a face W decomposes into a product of Boltzmann weights of bonds

$$W(\sigma_i, \sigma_j, \sigma_k, \sigma_l) = Q(\sigma_i, \sigma_j) Q(\sigma_j, \sigma_l) Q(\sigma_l, \sigma_k) Q(\sigma_k, \sigma_i). \tag{3.29}$$

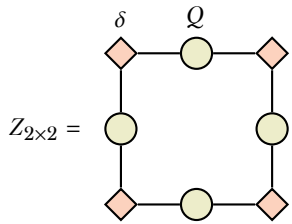

Figure 3.1: A tensor network representation of the partition function of the Ising model on a 2×2 lattice. See Eq. 3.30.

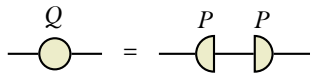

Figure 3.2: Graphical form of Eq. 3.32.

It is now easy to see that the partition function is equal to the contracted tensor network in Fig. 3.1:

$$\begin{aligned} Z_{2\times 2} &= \sum_{\sigma_1,\sigma_2,\sigma_3,\sigma_4} \sum_{a,b,c,d} \delta_{\sigma_1,a} Q(a,b) \delta_{\sigma_2,b} Q(b,c) \delta_{\sigma_3,c} Q(c,d) \delta_{\sigma_4,d} Q(d,a) \\ &= \sum_{\sigma_1,\sigma_2,\sigma_3,\sigma_4} W(\sigma_1,\sigma_2,\sigma_3,\sigma_4). \end{aligned} \tag{3.30}$$

where the Kronecker delta is defined as usual:

$$\delta_{ij} = \begin{cases} 1 & \text{if } i = j \\ 0 & \text{if } i \neq j. \end{cases} \tag{3.31}$$

3.3.2 Thermodynamic limit

We define the matrix P by

$$P^2 = Q. \tag{3.32}$$

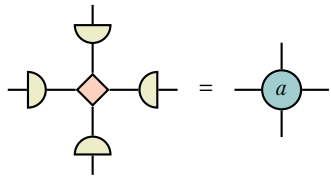

Figure 3.3: Graphical form of Eq. 3.33.

as in Fig. 3.2. This allows us to write the partition function of an arbitrary $N \times l$ square lattice as a tensor network of a single recurrent tensor a_{ijkl}, given by

$$a_{ijkl} = \sum_{a,b,c,d} \delta_{abcd} P_{ia} P_{jb} P_{kc} P_{ld}, \tag{3.33}$$

where the generalization of the Kronecker delta is defined as

$$\delta_{i_1 \ldots i_n} = \begin{cases} 1 & \text{if } i_1 = \ldots = i_n \\ 0 & \text{otherwise.} \end{cases} \tag{3.34}$$

See Fig. 3.3 and Fig. 3.4. At the edges and corners, we define suitable tensors of rank 3 and 2, which we will also denote by a:

$$a_{ijk} = \sum_{abc} \delta_{abc} P_{ia} P_{jb} P_{kc},$$
$$a_{ij} = \sum_{ab} \delta_{ab} P_{ia} P_{jb}.$$

The challenge is to approximate this tensor network in the thermodynamic limit.

3.3.3 The transfer matrix as a tensor network

Say something about reshaping legs. It is implicit now.

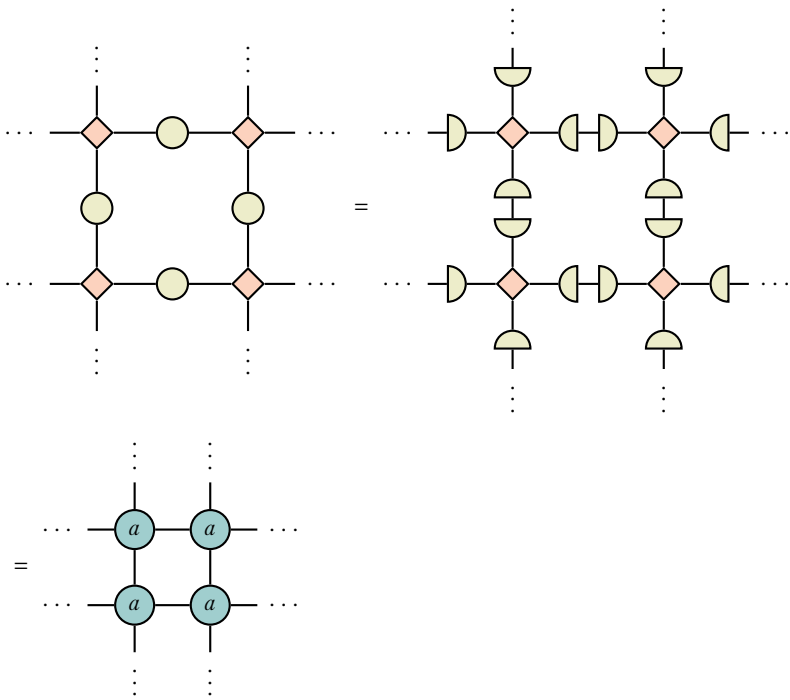

Figure 3.4: $Z_{N\times l}$ can be written as a contracted tensor network of $N \times l$ copies of the tensor a.

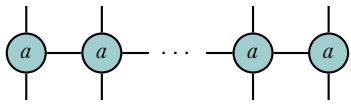

Figure 3.5: The definition of T_N as a network of N copies of the tensor a.

With our newfound representation of the partition function as a tensor network, we can redefine the row-to-row transfer matrix from Eq. 3.23 as the tensor network expressed in Fig. 3.5. For all l, it is still true that

$$Z_{N\times l} = \mathrm{Tr}\, T_N^l = \sum_{i=1}^{2^N} \lambda_i^l, \tag{3.35}$$

so the eigenvalues must be the same. That means that the new definition of the transfer matrix is related to the old one by a basis transformation

$$T_{\text{new}} = P T_{\text{old}} P^T. \tag{3.36}$$

3.4 Transfer matrix renormalization group

There is a deep connection between quantum mechanical lattice systems in d dimensions and classical lattice systems in $d+1$ dimensions. Via the imaginary time path integral formulation, the partition function of a one-dimensional quantum system can be written as the partition function of an effective two-dimensional classical system. The ground state of the quantum system corresponds to the largest eigenvector of the transfer matrix of the classical system.

For more on the quantum-classical correspondence, see Appendix A.

3.4.1 The infinite system algorithm for the transfer matrix

Nishino [9, 10] was the first to apply density matrix renormalization group methods in the context of two-dimensional classical lattices.

Analogous to the infinite system DMRG algorithm for approximating the Hamiltonian of quantum spin chains, our goal is to approximate the transfer matrix in the thermodynamic limit as well as possible within a restriced number of basis states m. We will do this by adding a single site at a time, and truncating the dimension from $2m$ to m at each iteration.

For simplicity, we assume that, at the start of the algorithm, the transfer matrix already has dimension m. We call this transfer matrix P_N. A good choice of initial transfer matrix is obtained by contracting a couple of a-tensors, until dimension m is reached. See Fig. 3.6.

To specify fixed instead of open boundary conditions, we may use as boundary tensor a slightly modified version of the three-legged version of a, namely

$$a^{\sigma}_{ijk} = \sum_{abc} \delta_{\sigma abc} P_{ia} P_{jb} P_{kc}, \tag{3.37}$$

that represents an edge site with spin fixed at σ.

We enlarge the system with one site by contracting with an additional a-tensor, obtaining P_{N+1}. See the first network in Fig. 3.7.

In order to find the best projection from $2m$ basis states back to m, we embed the system in an environment that is the mirror image of the system we presently have. We call this matrix T_{2N+2}. It represents the transfer matrix of $2N+2$ sites. We find the largest eigenvalue and corresponding eigenvector, as shown in Fig. 3.8.

The equivalent of the *reduced density matrix of a block* in the classical case is:

$$\rho_{N+1} = \sum_{\sigma_B} \langle \sigma_B | \lambda_0 \rangle \langle \lambda_0 | \sigma_B \rangle , \tag{3.38}$$

where we have summed over all the degrees of freedom of one of the half-row transfer matrices P_{N+1}. See the first step of Fig. 3.9.

The optimal renormalization

$$\widetilde{P}_{N+1} = O P_{N+1} O^{\dagger} \tag{3.39}$$

is obtained by diagonalizing ρ_{N+1} and keeping the eigenvectors corresponding to the m largest eigenvalues. See the second step of Fig. 3.9.

With this blocking procedure, we can successively find

$$P_{N+1} \to P_{N+2} \to \ldots, \tag{3.40}$$

until we have reached some termination condition.[2]

[2] The termination condition for the infinite-system algorithm is discussed in section 6.3.

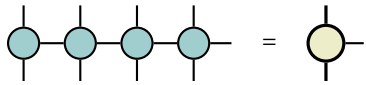

Figure 3.6: A good starting point for the half-row transfer P_N is obtained by contracting a couple of a-tensors, until P_N reaches dimension m.

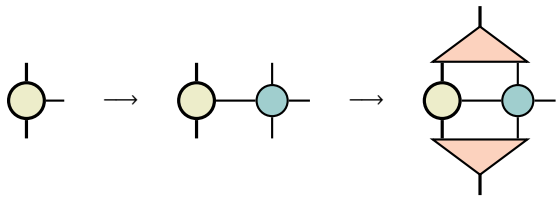

Figure 3.7: In the first step, P_{N+1} is obtained by contracting the current half-row transfer matrix P_N with an additional a-tensor. In the second step, P_{N+1} is truncated back to an m-dimensional matrix, with the optimal low-rank approximation given by keeping the basis states corresponding to the m largest eigenvalues of the density matrix. See Fig. 3.9.

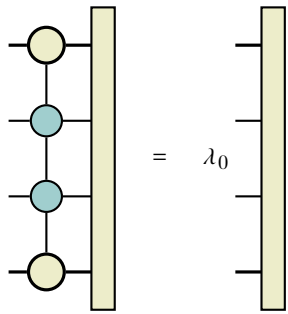

Figure 3.8: Equation for the lowest-lying eigenvector of the row-to-row transfer matrix T_{2N+2}.

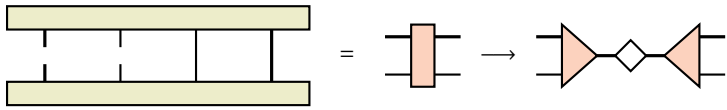

Figure 3.9: Graphical form of Eq. 3.38. In the second step, ρ_{N+1} is diagonalized and only the eigenvectors corresponding to the m largest eigenvalues are kept.

3.4.2 Physical interpretation of the reduced density matrix

Generalizing the remarks from section 3.2.1.1 to the two-dimensional case, we see that the normalized lowest-lying eigenvector of the transfer matrix T_N contains the Boltzmann weights of spin configurations on the boundary of a half-infinite $N \times \infty$ lattice.

Therefore, the classical equivalent of the quantum mechanical reduced density matrix, given by Eq. 3.38, and by the first network in Fig. 3.9, represents the Boltzmann weights of configurations along a cut in an $N \times \infty$ lattice.

Nishino and Okunishi [10], drawing on ideas from Baxter, realized the Boltzmann weights of configurations along this cut could be obtained by employing *corner transfer matrices*, making it unneccessary to solve the eigenvalue problem in Fig. 3.8. Their method, called the Corner Transfer Matrix Renormalization Group method, consumes far less resources while maintaining precision. For this reason, it is the method of choice for most of the simulations in this thesis.

3.5 Corner transfer matrix renormalization group

3.5.1 Corner transfer matrices

The concept of corner transfer matrices for 2D lattices was first introduced by Baxter [11–13]. Whereas the row-to-row transfer matrix Eq. 3.23 corresponds to adding a row to the lattice, the corner transfer matrix adds a quadrant of spins. It was originally defined by Baxter as

$$A_{\boldsymbol{\sigma},\boldsymbol{\sigma}'} = \begin{cases} \sum \prod_{\langle i,j,k,l \rangle} W(\sigma_i, \sigma_j, \sigma_k, \sigma_l) & \text{if } \sigma_1 = \sigma_1' \\ 0 & \text{if } \sigma_1 \neq \sigma_1'. \end{cases} \tag{3.41}$$

Here, the product runs over groups of four spins that share the same face, and the sum is over all spins in the interior of the quadrant.

In a symmetric and isotropic model such as the Ising model, we have

$$W(a, b, c, d) = W(b, a, d, c) = W(c, a, d, b) = W(d, c, b, a) \tag{3.42}$$

and the partition of an $N \times N$ lattice is expressed as

$$Z_{N\times N} = \mathrm{Tr}\, A^4. \tag{3.43}$$

In the thermodynamic limit, this partition function is equal to the partition function of an $N \times \infty$ lattice, given by Eq. 3.24.

The matrix in Eq. 3.38, containing the Boltzmann weights of spins along a cut down the middle of an $N \times \infty$ system, is *approximated* by

$$\rho = A^4. \tag{3.44}$$

The difference is that A^4 represents a square system of size $N \times N$ with a cut, instead of an $N \times \infty$ strip with a cut. In the thermodynamic limit, both systems become the same. In the corner transfer matrix renormalization group method, A^4 is used to find the optimal projector onto m basis states.

3.5.2 Corner transfer matrix as a tensor network

Similarly to how we redefined the row-to-row transfer matrix (Eq. 3.23) as the tensor network in Fig. 3.5, we can redefine the corner transfer matrix (Eq. 3.41) as the tensor network in Fig. 3.10. Again, the new and old definitions of A are related by a basis tranformation

$$A_{\text{new}} = P A_{\text{old}} P^T. \tag{3.45}$$

The partition function, as in Eq. 3.43, is given by the tensor network in Fig. 3.11.

3.5.3 Corner transfer matrix renormalization group method

The algorithm proceeds very much like the transfer matrix renormalization group method. In addition to renormalizing the half-row transfer matrix P, we also renormalize the corner transfer matrix A at each step, using the projector obtained from diagonalizing A^4.

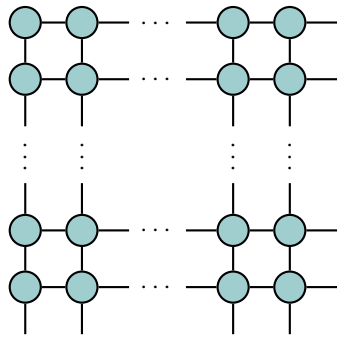

Figure 3.10: Corner transfer matrix expressed as a contraction of a-tensors.

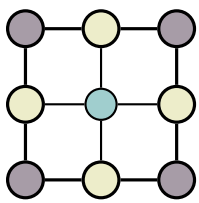

Figure 3.11: Tensor network approximation to $Z_{N\times N}$ in the CTMRG method.

Compare complexities of both algorithms?

We first initialize P_N and A_N, imposing boundary conditions as we see fit.

We then obtain the unrenormalized A_{N+1} by adding a layer of spins to the quadrant represented by A_N. This is done by contracting with two half-row transfer matrices P_N and a single a-tensor, as shown in the first step of Fig. 3.12. We obtain the unnormalized P_{N+1} as before, as shown in the first step of Fig. 3.7.

To find the optimal projector from $2m$ to m basis states, we can directly diagonalize A^4_{N+1}, or, equivalently, A_{N+1}. As always, we keep the basis states corresponding to the m largest eigenvectors. This is shown in Fig. 3.13. We use the projector to obtain the renormalized versions of A_{N+1} and T_{N+1}

$$\widetilde{A}_{N+1} = O A_{N+1} O^\dagger, \tag{3.46}$$

$$\widetilde{T}_{N+1} = O T_{N+1} O^\dagger. \tag{3.47}$$

shown in the second steps of Fig. 3.12 and Fig. 3.7.

We repeat the above procedure to successively obtain

$$A_{N+1} \to A_{N+2} \to \ldots, \tag{3.48}$$

$$T_{N+1} \to T_{N+2} \to \ldots \tag{3.49}$$

until a convergence criterion is reached.

3.6 Calculation of observable quantities

3.6.1 Free energy per site

Baxter [12, 13] showed that the partition function per site

$$\kappa = Z^{1/N^2} \tag{3.50}$$

is, within the corner transfer matrix renormalization group method, written as

$$\kappa = \frac{r_1 r_4}{r_2 r_3}, \tag{3.51}$$

with r_2, r_3 and r_4 as in Fig. 3.14 and $r_1 = Z_{N\times N}$ as in Fig. 3.11. The free energy per site is then simply

$$\frac{F}{N^2} = -T \log \kappa. \tag{3.52}$$

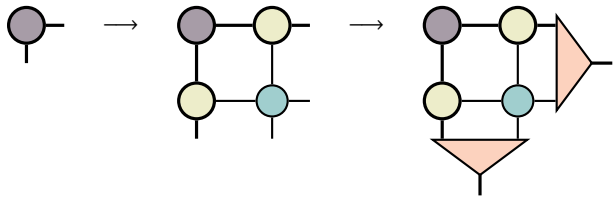

Figure 3.12: In the first step, the unrenormalized A_{N+1} is obtained by contracting with two copies of P_N and a single a-tensor. This corresponds to adding a layer of spins to the quadrant, thus enlarging it from $N \times N$ to $N+1 \times N+1$. In the second step, A_{N+1} is renormalized with the projector obtained from diagonalizing A^4_{N+1} and keeping the basis states corresponding to the m largest eigenvalues.

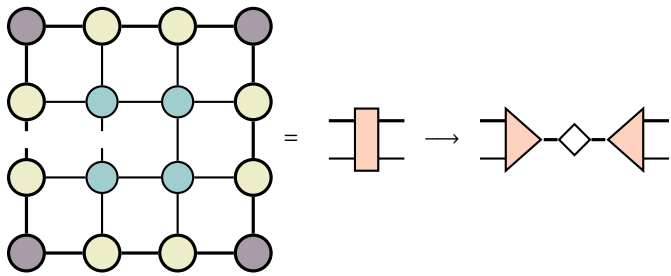

Figure 3.13: The matrix A^4_{N+1} is approximately equal to ρ_{N+1} in Eq. 3.38. Compare the graphical forms of this network and the one shown in Fig. 3.9. We obtain the optimal projector by diagonalizing A^4_{N+1}, or equivalently A_{N+1}.

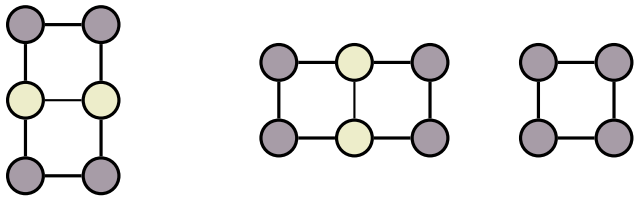

Figure 3.14: From left to right: r_2, r_3 and r_4 as in Eq. 3.51.

3.6.2 Magnetization per site

The magnetization per site may be calculated as

$$M = T\frac{\partial(\log \kappa)}{\partial h}, \tag{3.53}$$

but this involves a numerical derivative and a numerical limit $h \to 0$ in the case of the spontaneous magnetization. A more practical method, that is employed in this thesis, is to use the magnetization of the central spin

$$\langle \sigma_0 \rangle = \frac{\mathrm{Tr}\, A_+^4 - \mathrm{Tr}\, A_-^4}{\mathrm{Tr}\, A^4} \tag{3.54}$$

as a proxy quantity to the magnetization per site. Here, $A_\pm$ is the corner transfer matrix with the central spin fixed to $\pm$.

$\mathrm{Tr}\, A_+^4 - \mathrm{Tr}\, A_-^4$ is written as the tensor network in Fig. 3.15, with the tensor b_{ijkl} defined as

$$b_{ijkl} = \sum_{\sigma \in \{-1,1\}} \sigma \delta_{\sigma ijkl}. \tag{3.55}$$

All numerical results in this thesis involving the magnetization per site are actually obtained by calculating $\langle \sigma_0 \rangle$, which shall be referred to simply as M from now on.

3.6.3 Analogy to entanglement entropy for classical systems

The key point of the corner transfer matrix renormalization group method [10, 16] is that it unifies White's density matrix renormalization group method

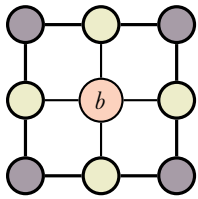

Figure 3.15: Unnormalized expectation value of central spin, with the tensor b_{ijkl} defined in Eq. 3.55.

[1] with Baxter's corner transfer matrix approach [11, 12], through the identification (in the isotropic case)

$$\rho_{\text{half-chain}} = A^4. \tag{3.56}$$

This allows one to define a 2D classical analogue to the half-chain entanglement entropy of a 1D quantum system

$$S_{\text{classical}} = -\operatorname{Tr} A^4 \log A^4 = -\sum_{\alpha=1}^{m} \nu_\alpha^4 \log \nu_\alpha^4, \tag{3.57}$$

where ν_α are the eigenvalues of the corner transfer matrix A. In the CTMRG algorithm, A is kept in diagonal form, making $S_{\text{classical}}$ trivial to compute.

In [17], numerical evidence is given for the validity of Eq. 3.57 for a wide range of models, and the concept is generalized to higher dimensions. For an overview of applying corner transfer matrices in higher dimensions and to quantum systems, see [18].

3.7 Spectrum of the corner transfer matrix

3.7.1 Analytical results for the Ising model

In what follows, we present results established in [19, 20].

For the off-critical Ising model on a square lattice, we have [21]

$$\hat{\rho} = \hat{A}^4 = \exp(-\hat{H}_{\text{CTM}}), \tag{3.58}$$

where

$$\hat{H}_{\mathrm{CTM}} = \sum_{l=0}^{\infty} \epsilon_l(T) c_l^\dagger c_l, \tag{3.59}$$

with c_l and $c_l^\dagger$ fermionic annihilation and creation operators and

$$\epsilon_l = \begin{cases} (2l+1)\epsilon(T) & \text{if } T > T_c, \\ 2l\epsilon(T) & \text{if } T < T_c. \end{cases} \tag{3.60}$$

with $\epsilon(T)$ a model-specific factor that only depends on temperature.

In other words, the reduced density matrix (or equivalently, the corner transfer matrix A) can be written as a density matrix of an effective free fermionic Hamiltonian with equally spaced excitations.

What does this mean for the spectrum of A? If we assume a free boundary, we have to distinguish between the ordered and disordered phase.

In the disordered phase, we have $\epsilon_l = (2l+1)\epsilon(T)$. The ground state, $E = 0$, corresponds to the vacuum state of the effective system described by H_{CTM}. The single-fermion excitations give ϵ, 3ϵ, 5ϵ, ..., while two-fermion excitations give 4ϵ ($c_0^\dagger c_1^\dagger |0\rangle$), 6ϵ ($c_0^\dagger c_2^\dagger |0\rangle$) and 8ϵ ($c_0^\dagger c_3^\dagger |0\rangle$ *or* $c_1^\dagger c_2^\dagger |0\rangle$). So the first degeneracy appears at 8ϵ. 9ϵ is also degenerate: it can be constructed with a single-fermion excitation ($c_4^\dagger |0\rangle$) and a three-fermion excitation ($c_2^\dagger c_1^\dagger c_0^\dagger |0\rangle$).

The numerical results from the CTMRG algorithm exactly confirm this picture. See the $T = 2.6$ line in the left panel of Fig. 3.16. The gap after the first two eigenvalues is due to the absence of the level 2ϵ. The ϵ_l are linear and the degeneracies are correct.

In the ordered phase, we have a two-fold degeneracy for every state due to symmetry and ground state energy $E = 0$. After that, the only available levels are 2ϵ, 4ϵ, 6ϵ, ... The degeneracy of the nth energy level is given by $2p(n)$, twice the number of partitions of n into distinct integers [22], with the factor of two coming from symmetry.

To illustrate: $c_1^\dagger c_2^\dagger |0\rangle$ and $c_3^\dagger |0\rangle$ both have $E = 6\epsilon$, the third energy level (counting the vacuum as the zeroth energy level), which is to say $p(3) = 2$ since $\{3, 2+1\}$ are the ways to write 3. The line $T = 2$ in the left panel of Fig. 3.16 confirms these results.

With a fixed boundary, the spectrum in the disordered phase doesn't change. In the ordered phase however, the two-fold degeneracy due to symmetry is lifted, so the degeneracy of the nth energy level becomes $p(n)$. As a consequence, the spectrum decays much faster. See the right panel of Fig. 3.16.

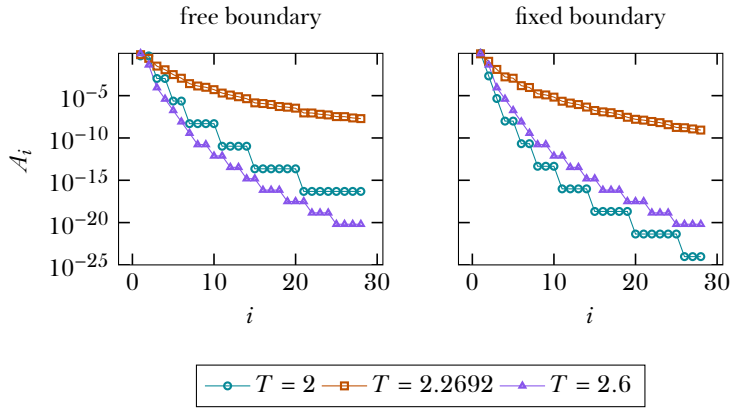

Figure 3.16: First part of the spectrum of A after $n = 1000$ steps with a bond dimension of $m = 250$.

At or close to criticality, the expression in Eq. 3.58 breaks down, and the spectrum of $\hat{\rho}$ is smoothened out. In general, below and at criticality, the spectrum decays slower for a free boundary. This is to be expected, since A preserves the symmetry when the boundary is free. At $T = 0$, A has two equally large non-zero eigenvalues, representing either all up or all down spins on the boundary of the quadrant, while for a fixed boundary, A has one non-zero eigenvalue: it represents a completely polarized state.

3.7.2 Implications for finite-m simulations

When approximating the corner transfer matrix with a free boundary in the ordered phase, it is crucial to retain all basis states corresponding to an energy level [22]. Failure to do so will lead to a symmetry-broken state.

Make this plot somewhere?

3.8 Equivalence to variational approximation in the space of matrix product states.

Talk about Baxter, Rommer and Ostlund, and more recent MPS algorithms. Maybe in appendix?

4

Critical behaviour and finite-size scaling

In this chapter, we introduce the central concepts in critical phenomena and finite-size scaling, largely following the review by Barber [23] and the less technical overview by Kadanoff [24].

4.1 Phase transitions

When matter exhibits a sudden change in behaviour, often characterized by a discontinuity or divergence of one or more thermodynamic quantities, we say it undergoes a *phase transition*.

A quantity that signifies this change is called an *order parameter*, which can take vastly different forms across systems and transitions. For example, for the transition of a ferromagnet, the order parameter is the net magnetization of the system, while for a percolation transition, it is the size of the largest connected graph.

For a historical account of the classification of phase transitions, see [25]. At the present time, we distinguish between two different types [24].

When some thermodynamic quantity changes discontinuously, i.e. shows a jump, we call the transition *first order*. In contrast, during a *continuous* phase transition a variable undergoes change continuously. The point at which a continuous phase transition occurs, is called the critical point.

The two-dimensional Ising model in a magnetic field shows both types of transition. At zero magnetic field and $T = T_c = 1/(\log(1 + \sqrt{2}))$, the magnetization changes from zero for $T > T_c$ to a finite value for $T < T_c$ in a continuous manner.

Below the critical temperature T_c, when the magnetic field h tends to zero from $h > 0$, the magnetization tends to a positive value. Conversely, when the magnetic field tends to zero from $h < 0$, the magnetization tends to a negative value. Thus, across the region $h = 0, T < T_c$ the system undergoes a first-order phase transition.

4.1.1 Finite systems

We will now argue that a phase transition cannot occur in a finite system, but only happens when the number of particles tends to infinity.

Because thermodynamic quantities are averages over all possible microstates of a system, those quantities are completely defined in terms of the system's partition function, or equivalently its free energy.

Since in a finite system, the partition function is a finite sum of exponentials, it is analytic (infinitely differentiable). Hence, thermodynamic quantities cannot show true discontinuities and the phase transitions described in the above section do not occur.

4.2 Critical behaviour

We will now focus our attention on continuous phase transitions, more specifically the one that occurs in the two-dimensional Ising model. Before we discuss the behaviour of the free energy around the critical point, we briefly summarize how the thermodynamic limit is approached far away from it. Here, we largely follow [23].

We assume that the free energy per site in the thermodynamic limit

$$f_\infty(T) = \lim_{N\to\infty} \frac{F(T,N)}{N} \tag{4.1}$$

exists, and is not dependent on boundary conditions. By definition, it is not analytic in a region around the critical point.

Outside that region, however, we can write

$$F(T,N) = N f_\infty(T) + o(N), \tag{4.2}$$

where correction terms $g(N)$ of $o(N)$ (little-o of N) obey

$$\lim_{N\to\infty} \frac{g(N)}{N} = 0. \tag{4.3}$$

These corrections, of course, do depend on boundary conditions.

Eq. 4.2 is valid only outside the critical region precisely because $F(T,N)$ is analytic *everywhere*, and $f_\infty(T)$ is only analytic away from the critical point.

The behaviour of $F(T,N)$ (and hence, all thermodynamic quantities) at criticality is approached is described by *finite-size scaling*.

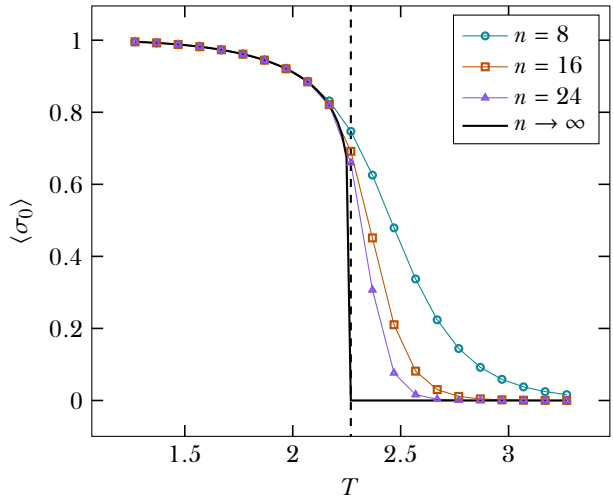

Figure 4.1: The magnetization of the central spin for small lattices with boundary spins fixed to +1. The black line is the exact solution in the thermodynamic limit.

4.2.1 Finite-size scaling

Fig. 4.1 shows the behaviour of the order parameter obtained by exact diagonalization of the partition function of small lattices. It is clear that far from the critical point, the order parameter is essentially not dependent on system size, while in critical region there are significant deviations from the thermodynamic behaviour.

One can now define two characteristic temperatures [23, 26]. The first being the cross-over temperature T_X at which finite-size effects become important, which is predicted to scale as

$$|T_X - T_c| \propto N^{-\theta}. \tag{4.4}$$

θ is called the cross-over or rounding exponent.

The second characteristic temperature is the pseudocritical temperature, denoted by $T^\star$. It can be defined in several ways, one being the point where

the order parameter becomes almost zero, or the point where the heat capacity

$$C = T^2 \frac{\partial^2 F}{\partial T^2} \tag{4.5}$$

reaches its maximum. $T^\star$ can be regarded as the point where the finite system in some sense comes closest to undergoing a transition.

Generally $T^\star$ will not equal T_X. Furthermore, $T^\star$ depends on boundary conditions: periodic or fixed boundary conditions will nudge the system into an ordered state, therefore $T^\star > T_c$. Free boundary conditions will cause the system to favor disorder and the pseudocritical temperature to be lowered.

In any case, it is predicted that

$$|T^\star - T_c| \propto N^{-\lambda}. \tag{4.6}$$

It is generally accepted that [23]

$$\lambda = \theta. \tag{4.7}$$

Furthermore, if one assumes that finite-size effects become important once the correlation length of the system becomes of order of the system size, i.e. [26]

$$\xi(T_X(N)) \propto N, \tag{4.8}$$

then the correlation length exponent ν, given by

$$\xi(T) \propto |T - T_c|^{-\nu} \tag{4.9}$$

is, by using Eq. 4.4, related to θ as

$$\theta = \frac{1}{\nu}. \tag{4.10}$$

4.2.1.1 The finite-size scaling ansatz

The behaviour of a system of finite size N is expected to be a function of the ratio

$$y = \frac{N}{\xi(T)}, \tag{4.11}$$

where $\xi(T)$ is the correlation length of the thermodynamic system [27].

With the assumption in Eq. 4.8, this means that in the limit $y \gg 1$, we expect to see thermodynamic behaviour, while for $y \ll 1$, the finite system size should enter in the analysis.

To see exactly how this happens, consider as an example the order parameter M, which in the thermodynamic limit, close to the critical point obeys

$$M(T) \propto \begin{cases} (-t)^{\beta} & \text{if } T \leq T_c, \\ 0 & \text{if } T \geq T_c, \end{cases} \tag{4.12}$$

where we have defined the reduced temperature

$$t = \frac{T - T_c}{T_c}. \tag{4.13}$$

Assuming the correlation length diverges algebraically

$$\xi(T) \propto |t|^{-\nu}, \tag{4.14}$$

for $T < T_c$ we have

$$M(T) \propto \xi(T)^{-\beta/\nu}. \tag{4.15}$$

The *finite-size scaling ansatz* now says that for finite systems

$$M(T, N) = N^{-\beta/\nu} \mathcal{F}(y), \tag{4.16}$$

with the requirement that for $N \to \infty$, it should reproduce the thermodynamic behaviour in Eq. 4.15, leading to

$$\lim_{y \to \infty} \mathcal{F}(y) \propto y^{\beta/\nu}. \tag{4.17}$$

At the critical point, however, the bulk correlation length diverges and the only relevant length scale is N, so that we must have

$$M(T = T_c, N) \propto N^{-\beta/\nu}, \tag{4.18}$$

from which it follows that

$$\lim_{y \to 0} \mathcal{F}(y) = \text{const.} \tag{4.19}$$

4.2.1.2 Extracting exponents from numerical simulation

To extract critical exponents from (finite) numerical simulations, Eq. 4.16 may be written as

$$M(T, N) = N^{-\beta/\nu}\mathcal{G}(tN^{1/\nu}) \tag{4.20}$$

where it is used that (per Eq. 4.14)

$$y = \frac{N}{\xi(T)} \propto t^{\nu}N, \tag{4.21}$$

and the new scaling function is customarily written as having argument $tN^{1/\nu} = (t^{\nu}N)^{1/\nu}$.

The critical exponents β and ν and the critical temperature can now be extracted by asserting that the numerical data for different system sizes should collapse on a single curve

$$\mathcal{G}(tN^{1/\nu}) = M(T, N)N^{\beta/\nu}. \tag{4.22}$$

The authors of [28] propose a measure of the fitness $P(\beta, \nu, T_c)$ of such a data collapse

$$P(\beta, \nu, T_c) = \frac{1}{\mathcal{N}_{\text{overlap}}} \sum_{p} \sum_{j \neq p} \sum_{i_{\text{overlap}}} |M(t_{ij}, N_j)N_j^{\beta/\nu} - \mathcal{C}_p(t_{ij}N_j^{1/\nu})|, \tag{4.23}$$

where for each system size N_p, the data points collected for the other system sizes N_j that overlap (that is, fall between any two data points collected for N_p) are compared with the interpolation $\mathcal{C}_p(t_{ij}N_j^{1/\nu})$ between those two data points. $\mathcal{N}_{\text{overlap}}$ is the number of overlapping pairs.

It is clear that

$$P(\beta, \nu, T_c) \geq 0 \tag{4.24}$$

and the optimal values for β, ν and T_c minimize $P(\beta, \nu, T_c)$.

This measure for the data collapse is found, for data collected for this thesis, to work significantly better than other proposed measures such as fitting a polynomial or order 3-8 through all data points.

5
Finite-m scaling in the CTMRG algorithm

The connection between finite-size scaling, as introduced in the last chapter, and finite-size effects as a consequence of the finite bond dimension m within the CTMRG algorithm is made.

We discuss ideas by Nishino [29], who was the first to investigate these effects, by linking the finite-bond dimension m to the inherently finite correlation length of the approximated system at the critical point. These ideas were later made more precise via the connection of the CTMRG algorithm in the thermodynamic limit to matrix product states [12, 30], which inherently have a finite correlation length [31, 32].

Then, we discuss a more recent theory of finite-entropy scaling, developed in [33] (earlier numerical evidence was given in [34, 35]), which implies a scaling of the correlation length for a matrix product state with finite bond dimension of the form $\xi \propto m^{\kappa}$.

5.1 Introduction

Up until now, we have developed our scaling analysis in terms of a finite system size N. But the approximation of the infinite-system partition function with the CTMRG algorithm depends on two parameters; the system size N and the bond dimension m.

A finite bond dimension m carries a characteristic length scale. Baxter [12], and later Östlund and Rommer [30] (in the context of one-dimensional quantum systems) showed that in the thermodynamic limit, CTMRG and DMRG are variational optimizations in the space of matrix product states.

Can extend this idea a bit.

It is known that an MPS-ansatz with finite bond dimension inherently limits the correlation length of the system to a finite value [31, 32]. Hence, thermodynamic quantities obtained from the CTMRG algorithm with finite m, in

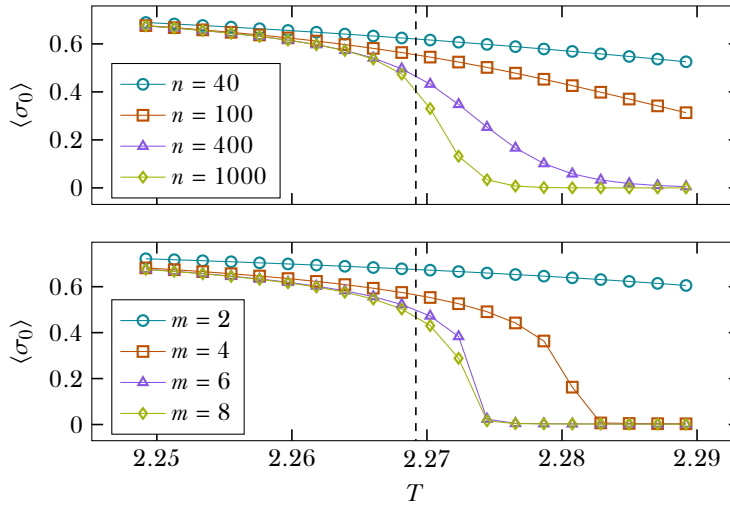

Figure 5.1: Upper panel: expectation value of the central spin $\langle\sigma_0\rangle$ after n CTMRG steps. m is chosen such that the truncation error is smaller than 10^{-6}. Lower panel: $\langle\sigma_0\rangle$ for systems with bond dimension m.

the limit $N \to \infty$, cannot diverge and must show finite-size effects similar to those of some effective finite system of size $N_{\text{eff}}(m)$ depending on the bond dimension m.

Fig. 5.1 shows the behaviour of the order parameter of the two-dimensional Ising model for systems of finite-size, where the result is converged in m, and for systems of finite m, where the result is converged in the system size N. The results look very similar and support the claim that there are two relevant length scales in the critical region, namely the system size N and the length scale associated to the finite bond dimension m.

5.2 Definition of the effective length scale in terms of the correlation length at T_c

The first direct comparison of finite-size scaling in the system size N with scaling in the bond dimension of the CTMRG method m was done in [29].

In the thermodynamic limit (corresponding to infinite m and N), we have the following expression for the correlation length of a classical system [36]

$$\xi(T) = \frac{1}{\log\left(\frac{T_0}{T_1}\right)}. \tag{5.1}$$

Here, T_0 and T_1 are the largest and second-largest eigenvalues of the row-to-row transfer matrix T, respectively. With N tending towards infinity and finite m, near the critical point $\xi(T)$ should obey a scaling law of the form

$$\xi(T, m) = N_{\text{eff}}(m)\mathcal{F}(N_{\text{eff}}(m)/\xi(T)) \tag{5.2}$$

with

$$\mathcal{F}(x) = \begin{cases} \text{const} & \text{if } x \to 0, \\ x^{-1} & \text{if } x \to \infty. \end{cases} \tag{5.3}$$

Hence, the effective length scale corresponding to the finite bond dimension m is proportional to the correlation length of the system at the critical point $t = 0$.

$$N_{\text{eff}}(m) \propto \xi(T = T_c, m). \tag{5.4}$$

Look ahead to replicating this in results section?

5.3 Relation to finite-entropy scaling and the exponent κ.

The first numerical evidence of a law for the correlation length at the critical point of the form

$$\xi(m) \propto m^{\kappa} \tag{5.5}$$

was given by the authors of [35], who found

$$\kappa \approx 1.3 \tag{5.6}$$

for a gapless system of free fermions, using DMRG calculations. Later, using the iTEBD algorithm [37], the authors of [34] presented numerical evidence

for such a relation for the Ising model with transverse field and the Heisenberg model, with

$$\kappa_{\text{Ising}} \approx 2, \tag{5.7}$$

$$\kappa_{\text{Heisenberg}} \approx 1.37. \tag{5.8}$$

5.3.1 Quantitative theory for κ

A quantitative theory of the existence of an exponent κ was given in [33]. We reproduce the argument, which is presented in the language of one-dimensional quantum systems, below.

We start by noting that in the critical region, the entanglement of a half-infinite subsystem A diverges as

$$S_A \propto \mathcal{A}(c/6)\log(\xi), \tag{5.9}$$

where $\mathcal{A}$ is the number of boundary points of A and c is the central charge of the conformal field theory at the critical point [38–40].

Recalling the definition of the entanglement entropy

$$S_A = -\operatorname{Tr}(\rho_A \log \rho_A) = -\sum_\alpha \omega_\alpha \log \omega_\alpha, \tag{5.10}$$

it is trivially seen that the entropy of a state given by the DMRG (or any other MPS), which only retains m basis states of ρ_A, is limited by

$$S_A^{\max}(m) = \log m \tag{5.11}$$

by putting $\omega_\alpha = 1/m$ for $\alpha = 1, \ldots, m$.

This is, incidentally, another way to see that DMRG or CTMRG, or any other algorithm which produces ground states with a matrix-product structure have an inherently finite correlation length.

The leading energy correction to the free energy per site of a one-dimensional quantum system at a conformally invariant critical point at finite temperature T in the thermodynamic limit is [41]

$$f(T) = f_0 + aT^2 + \mathcal{O}(T^3). \tag{5.12}$$

Due to the quantum-classical correspondence, this is equivalent to a two-dimensional classical $N \times \infty$ lattice with strip width $N = 1/T$. This implies

also that the correlation length of a critical one-dimensional quantum system at finite temperature cannot diverge and goes as $\xi \propto 1/T$. In terms of this finite correlation length, Eq. 5.12 is written as

$$f(\xi) = f_\infty + \frac{A}{\xi^2} + \mathcal{O}(\frac{1}{\xi^3}). \tag{5.13}$$

Empirically, optimized ground states with a matrix-product structure at criticality do not simply maximize their entropy, as they should if we take Eq. 5.13 to be true for ground states with a matrix-product structure.

We will now show that Eq. 5.13 needs, in fact, an additional term due to the matrix-product structure with finite bond dimension m.

The ground state with finite correlation length and energy density as in Eq. 5.13 has a Schmidt decomposition that in principle can have infinitely many terms

$$|\psi_0\rangle = \sum_{n=1}^{\infty} \lambda_n \, |\psi_n^L\rangle \, |\psi_n^R\rangle \,, \tag{5.14}$$

where $|\psi_n^L\rangle$ and $|\psi_n^R\rangle$ are states of the left and right infinite half-chains. Normalization requires

$$\sum_{n}^{\infty} \lambda_n^2 = 1. \tag{5.15}$$

The ground state with a matrix-product structure with finite bond dimension m has an additional constraint: its Schmidt decomposition carries only the m $|\psi_n\rangle$ with largest λ_n. It is written as

$$|\psi_0^{\mathrm{MPS}}\rangle = \frac{\sum_{n=1}^{m} \lambda_n \, |\psi_n^L\rangle \, |\psi_n^R\rangle}{\sqrt{\sum_{n=1}^{m} \lambda_n^2}}. \tag{5.16}$$

To find the extra energy cost of only keeping the first m terms in the Schmidt decomposition, note that in the limit of m large, $|\psi_0^{\mathrm{MPS}}\rangle$ almost entirely overlaps with $|\psi_0\rangle$, hence can be written as

$$|\psi_0^{\mathrm{MPS}}\rangle = \sqrt{1-\epsilon^2} \, |\psi_0\rangle + \epsilon \, |\psi_{\mathrm{ex}}\rangle \,, \tag{5.17}$$

where $|\psi_{\mathrm{ex}}\rangle$ is some excited state and $\epsilon \ll 1$. This leads to an energy of

$$E_0^{\mathrm{MPS}} = \langle \psi_0^{\mathrm{MPS}} | \hat{H} | \psi_0^{\mathrm{MPS}} \rangle = E_0 + \epsilon^2 (E_{\mathrm{ex}} - E_0), \tag{5.18}$$

with

$$\epsilon^2 = \left(1 - \langle\psi_0|\psi_0^{\mathrm{MPS}}\rangle^2\right) = 1 - \sum_{n=1}^{m} \lambda_n^2 \equiv P_{\mathrm{res}}(m). \tag{5.19}$$

Here, we have defined the residual probability P_{res}, also known as the truncation error, as the part of the spectrum that is thrown away.

If we now assume that $E_0 - E_{\mathrm{ex}}$ is proportional to the energy gap Δ, which scales as [42–44]

$$\Delta \propto \frac{1}{\xi}, \tag{5.20}$$

we arrive at

$$E_0^{\mathrm{MPS}} = E_\infty + \frac{A}{\xi^2} + \frac{BP_{\mathrm{res}}(m)}{\xi}. \tag{5.21}$$

It is clear that when the correlation length is very large, by Eq. 5.9 the entropy and $P_{\mathrm{res}}(m)$ must be too. So, the third term in Eq. 5.21 dominates.

If the correlation length is small, the second term dominates. The correlation length that belongs to the MPS ground state with fixed m is the optimum that minimizes this expression.

The details of the calculation, which can be found in the supplementary material of [33], depend on the asymptotic form of P_{res}, found in [45]. In the limit $m \to \infty$, the correlation is indeed of the form in Eq. 5.5 with

$$\kappa = \frac{6}{c\left(\sqrt{12/c} + 1\right)}, \tag{5.22}$$

which is in good agreement with the values found in [34].

5.4 Locating the critical point with the entanglement spectrum

Since phase transitions of quantum systems can be located by studying their entanglement spectrum [17, 46], classical systems may be investigated in the same way through the correspondence in Eq. 3.56. This is an alternative to the usual approach of studying an order parameter or derivatives of thermodynamical observables.

Examples of studies using the spectrum of the corner transfer matrix to analyze two-dimensional classical systems are [47–49].

At the critical point, the entropy must diverge (cf. Eq. 5.9). For finite systems the entropy will remain finite, but the pseudocritical temperature $T^\star$ is defined as the point of maximum entropy. The critical point is then located by fitting the scaling law in Eq. 4.6.

6
Methods

We describe the technical details of the algorithms used to compute quantities of interest. We report the convergence behaviour of the algorithms and discuss validity and sources of error.

6.1 Symmetricity and normalization of tensors

For the models treated in this thesis, the corner transfer matrix A and the row-to-row transfer matrix T are symmetric. But due to the accumulation of machine-precision sized errors in the matrix multiplication and singular value decomposition, this will, after many algorithm steps, no longer be the case. In order for results to remain valid, we manually enforce symmetricity after each step.

The tensor network contractions at each algorithm step will cause the elements of A and T to tend to infinity, which means that they will at some point exceed the maximum value of a floating point number as it can be stored in memory. But because the elements of A and T represent Boltzmann weights, they can be scaled by a constant factor, which allows us to prevent this overflow if we use a suitable scaling. For example by requiring that

$$\mathrm{Tr}\, A^4 = 1, \tag{6.1}$$

so that the interpretation of A^4 as a reduced density matrix of an effective one-dimensional quantum is valid.

6.2 Boundary conditions

Unless otherwise stated, all simulations are run with the boundary spins of the lattice fixed to +1. For specific purposes, free boundary conditions are used.

6.3 Convergence criteria

6.3.1 Simulations with finite bond dimension

The convergence of the CTMRG algorithm with fixed bond dimension m (the infinite system algorithm) can be defined in multiple ways (*cite*). In this thesis, the convergence after step i of the algorithm is defined as

$$c_i = \sum_{\alpha=1}^{m} |s_\alpha^{(i)} - s_\alpha^{(i-1)}|, \tag{6.2}$$

where s_α are the singular values of the corner transfer matrix A. If the convergence falls below some threshold ϵ, the algorithm terminates.

The assumption is that once the singular values stop changing to some precision, the optimal projection is sufficiently close to its fixed point and the transfer matrices A and T represent an environment only limited by the length scale given by m, i.e.

$$\xi(m) \ll N \tag{6.3}$$

is satisfied.

6.3.1.1 Convergence at the critical point of the Ising model

The convergence is shown in Fig. 6.1. It is clear that the phenomenological law

$$\log c_n \propto n \tag{6.4}$$

holds to high precision, with the slope depending on m. Deviations only occur at values of c of around 10^{-12}.

The convergence of the various quantities as function of the number of algorithm steps is shown in Fig. 6.2. For all quantities Q, the absolute value of the relative difference with the final algorithm step

$$\Delta Q_{\text{rel}}(n) = \left| \frac{Q(n) - Q(n = 10^5)}{Q(n = 10^5)} \right| \tag{6.5}$$

is shown. Again, a law of the form

$$\log(\Delta Q_{\text{rel}}) \propto n \tag{6.6}$$

seems to hold.

To make an estimate of a quantity in the limit $N \to \infty$, or equivalently $\epsilon \to 0$, we can study the change in a quantity as function of the convergence threshold ϵ. We define

$$\Delta Q_{\text{step}}(\epsilon) = Q(\epsilon) - Q(10\epsilon), \tag{6.7}$$

i.e. the change of quantity Q when we decrease the threshold ϵ by an order of magnitude. The results in Fig. 6.3 show that, the order parameter, entropy and correlation length to high precision follow the linear relationship

$$\Delta Q_{\text{step}}(\epsilon) = \alpha_Q(m)\epsilon, \tag{6.8}$$

whereas the free energy follows a quadratic relationship

$$\Delta f(\epsilon) = \alpha_f(m)\epsilon^2. \tag{6.9}$$

Why is this case? It must have something to do with the fact that in the definition of the free energy the log is taken.

This means that we can confidently extrapolate the value of a quantity in the fully converged limit as

$$Q(\epsilon \to 0) = Q(\epsilon_{\min}) + \sum_{\epsilon = \frac{\epsilon_{\min}}{10}, \frac{\epsilon_{\min}}{100}, \ldots} \Delta Q_{\text{step}}(\epsilon), \tag{6.10}$$

where $\epsilon_{\min}$ is the lowest threshold used in simulation, and $\Delta Q_{\text{step}}(\epsilon)$ is determined by fitting to suitable higher values of the threshold.

6.3.2 Simulations with finite system size

In the finite-system algorithm, we want to reliably extrapolate quantities in the bond dimension m. The convergence behaviour is shown in Fig. 6.4. For each quantity Q, we plot the absolute value of the relative difference with the value at the highest m

$$\Delta Q_{\text{rel}}(m) = \left| \frac{Q(m) - Q(m = 200)}{Q(m = 200)} \right| \tag{6.11}$$

versus the bond dimension m.

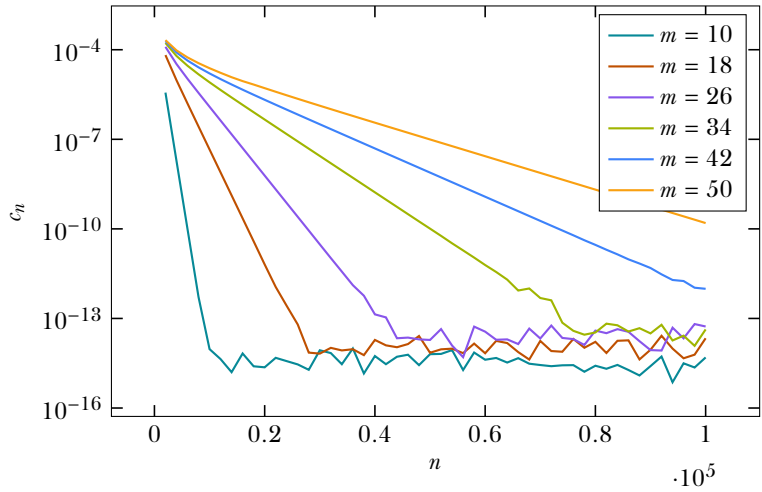

Figure 6.1: Convergence as defined in Eq. 6.2 versus n, the number of CTMRG steps. Up until very small values of c_n, the convergence is monotonically decreasing and obeys a logarithmic law with slope depending on m.

The plateaus of m-values that barely increase the precision are due to the structure in the spectrum of the reduced density matrix. Apart from this noise, the law

$$\Delta Q_{\text{rel}}(m) \propto m^{\alpha(N)} \tag{6.12}$$

is seen to hold for high enough m for the order parameter, free energy and entropy.

To extrapolate to $m \to \infty$, analogously to the finite-m case we define

$$\Delta Q_{\text{step}}(m) = Q(m) - Q(m-1), \tag{6.13}$$

which is plotted in the left panel of Fig. 6.5. As expected from Eq. 6.12, the overall trend looks like a power law, but the noise makes it hard to determine it accurately. It is anyway neither practical nor needed to calculate a system of finite size for many consecutive values of m, in order to get a good approximation to Eq. 6.13. Instead, one might compute the quantity for equally spaced values of m with a difference of say, 10 or 20.

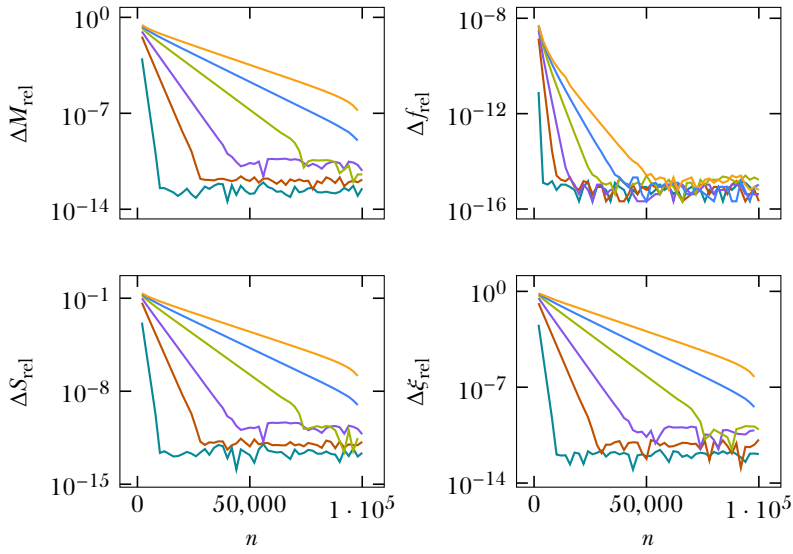

Figure 6.2: Absolute value of relative difference of quantities (see Eq. 6.5). Same legend as Fig. 6.1.

As described in section 3.7 and in [19, 21, 22], for the off-critical Ising model the degeneracies in the corner transfer matrix A are exactly known. These degeneracies are smoothed out, but not completely lost for finite systems near criticality. This is directly related to the convergence of quantities in m.

As an alternative to Eq. 6.13, it might be conjectured that not a fixed increase of m, but taking all basis states corresponding to the next energy level will increase accuracy in a predictable way.

This suspicion is confirmed in the right panel of Fig. 6.5, which shows the convergence using only the values of m for which all basis states with a certain

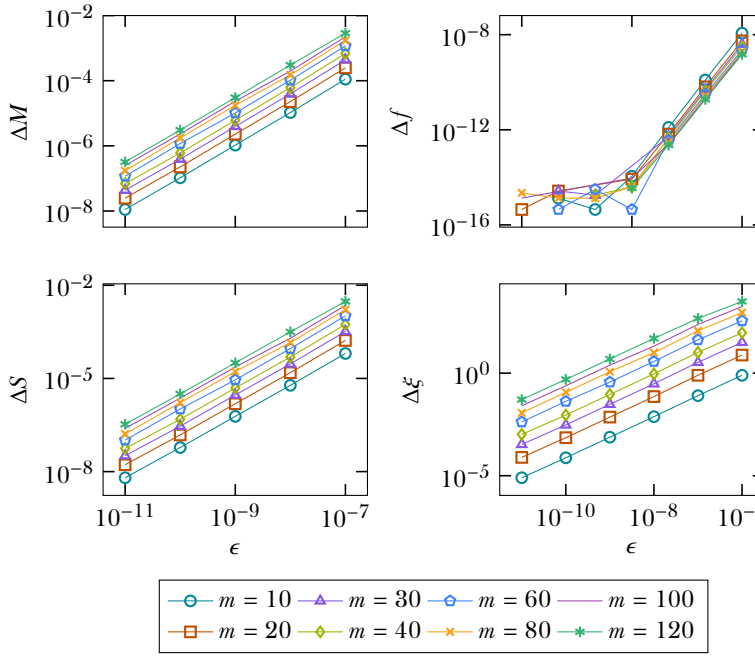

Figure 6.3: Stepwise differences upon decreasing the threshold ϵ by an order of magnitude, as in Eq. 6.7. For the order parameter, entropy and correlation length, a linear relationship holds to high precision, while for the free energy the relationship is quadratic.

energy level are present, i.e. [22]

$$m(j) = \sum_{k=0}^{k=j} p(k). \tag{6.14}$$

The first few values of $m(j)$ are

$$1, 2, 3, 5, 7, 10, 14, 19, 25, 33, 43, 55, 70, 88, 110, 137, 169, 207, \ldots \tag{6.15}$$

Using these values of m, the result is again a power law, and the noise largely disappears, but the convergence behaviour is still not devoid of structure entirely.

The error on a quantity calculated at bond dimension $m_{\max}$ can be approximated as

$$M(m \to \infty) = M(m_{\max}) + \sum_{\text{higher values of } m} \Delta Q_{\text{step}}(m), \tag{6.16}$$

where ΔQ_{step} is fitted from aptly chosen lower values of m.

6.4 Values of hyperparameters for the Ising model

We have found that for practical purposes, in the infinite-system algorithm the convergence threshold ϵ may be set to 10^{-7} for values of m below, say, 30, and to 10^{-8} for m-values above 40. For the highest value of $m = 120$, this leads to a relative error, as compared with the theoretically fully converged limit $\epsilon \to 0$, of about 0.1% in the correlation length, and less than 0.02% in the order parameter, entropy and free energy (the relative error on the free energy being basically zero). For lower values of m, the relative errors are substantially lower. See Table 6.1.

What about convergence at $T^\star$?

For simulations of finite systems, we have found that choosing m such that the truncation error P_r (for *residual probability*, its other common name) is smaller than 10^{-6} is sufficient for most purposes. This leads to a relative error with the fully converged limit $m \to \infty$ of at most 0.06% in the order parameter, entropy and free energy for $n = 8000$. For lower values of N, the relative error is lower. Here, we have taken the order parameter as the main benchmark, since the correlation length is not used for finite-size calculations. See Table 6.2.

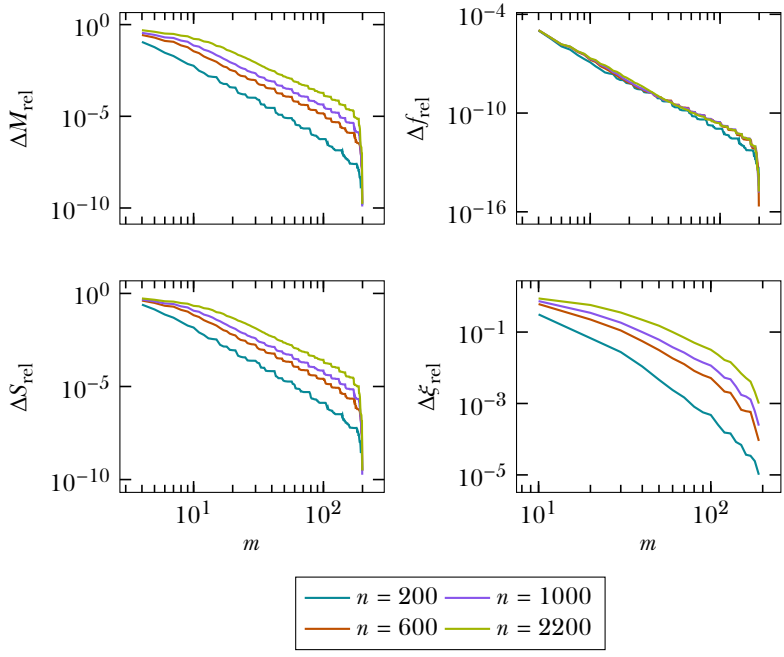

Figure 6.4: The absolute value of the relative difference of quantities, as defined in Eq. 6.11. For high enough m, it obeys a power law with varying exponent $\alpha(N)$. The sharp drop for the highest values of m is an artefact of the definition of ΔQ_{rel} and the plateau-like fashion in which the value of a quantity converges, owing to the spectrum of the reduced density matrix approximated by the CTMRG algorithm. Like in the finite-m case, the free energy converges much faster than the other quantities, and does so with little n-dependence. Note that $\Delta\xi_{\mathrm{rel}}$ does not obey a power law.

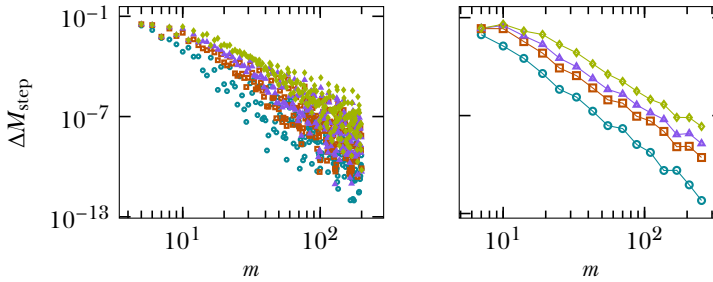

Figure 6.5: Same legend as Fig. 6.4

m	rel. error % ($\epsilon = 10^{-7}$)	rel. error % ($\epsilon = 10^{-8}$)
40	0.02	0.02
80	0.6	0.05
120	1.1	0.1

Table 6.1: Relative errors of $\xi(T_c, m, \epsilon)$, as compared with the fully converged limit $\epsilon \to 0$, approximated by Eq. 6.10.

n	rel. error % ($P_r < 10^{-5}$)	rel. error % ($P_r < 10^{-6}$)	rel. error % ($P_r < 10^{-7}$)
1000	0.08 (40)	0.005 (80)	0.001 (120)
2000	0.08 (60)	0.008 (100)	0.002 (160)
8000	0.6 (80)	0.07 (140)	0.005 (280)

Table 6.2: Relative errors of $M(T_c, n)$, calculated such that the truncation error P_r does not exceed listed threshold, as compared with the fully converged limit of $m \to \infty$ (zero truncation error), approximated by Eq. 6.16. The number in brackets is the value of m used. To approximate the error, steps in m-value of 5, 10 or 20 were used, depending on $m_{\max}$.

7
Numerical results for the Ising model

We present numerical results of finite-m and finite-size scaling within the CTMRG method on the Ising model.

7.1 At the critical point

7.1.1 Existence of two length scales

First, we reproduce the results presented in [29] to validate the assumption that at the critical point, the only relevant length scales are the system size N and the length scale associated to a finite dimension m of the corner transfer matrix $\xi(m)$. Here, we assume that $\xi(m)$ is given by the correlation length at the critical point, see section 5.2.

The order parameter[1] should obey the following scaling relation at the critical temperature

$$M(T = T_c, m) \propto \xi(T = T_c, m)^{-\beta/\nu}. \tag{7.1}$$

The left panel of Fig. 7.1 shows that this scaling relation holds. The fit yields $\frac{\beta}{\nu} \approx 0.125(5)$, close to the true value of $\frac{1}{8}$.

The right panel shows the conventional finite-size scaling relation

$$M(T = T_c, N) \propto N^{-\beta/\nu}, \tag{7.2}$$

yielding $\beta/\nu \approx 0.1249(1)$.

The correlation length $\xi(m)$ shows characteristic half-moon patterns on a log-log scale, stemming from the degeneracies in the corner transfer matrix spectrum. This makes the data harder to interpret, since the effect of increasing m depends on how much of the spectrum is currently retained.

[1] It is worth stressing that the order parameter and the magnetization per site are used interchangeably for the Ising model, and that the magnetization per site is approximated, within the CTMRG algorithm, by the expectation value of the central spin. See section 3.6.2.

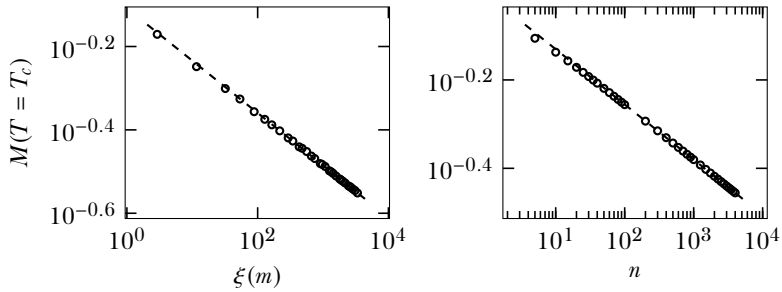

Figure 7.1: Left panel: fit to the relation in Eq. 7.1, yielding $\frac{\beta}{\nu} \approx 0.125(5)$. The data points are obtained from simulations with $m = 2, 4, \ldots, 64$. The smallest 10 values of m have not been used for fitting, to diminish correction terms to the basic scaling law. Right panel: fit to conventional finite-size scaling law given in Eq. 7.2, fitted with $n = 1500, 1750, \ldots, 4000$, calculated with a truncation error no larger than 10^{-7}, yielding $\beta/\nu \approx 0.1249$.

To further test the hypothesis that N and $\xi(m)$ are the only relevant length scales, the authors of [29] propose a scaling relation for the order parameter M at the critical temperature of the form

$$M(N, m) = N^{-\beta/\nu} \mathcal{G}(\xi(m)/N) \tag{7.3}$$

with

$$\mathcal{G}(x) = \begin{cases} \text{const} & \text{if } x \to \infty, \\ x^{-\beta/\nu} & \text{if } x \to 0, \end{cases} \tag{7.4}$$

meaning that Eq. 7.3 reduces to Eq. 7.2 in the limit $\xi(m) \gg N$ and to Eq. 7.1 in the limit $N \gg \xi(m)$. Fig. 7.2 shows that the scaling relation of Eq. 7.3 is justified.

Fig. 7.3 shows the cross-over behaviour from the N-limiting regime, where $M(N, m) \propto N^{-\beta/\nu}$ to the $\xi(m)$-limiting regime, where $M(N, m)$ does not depend on N.

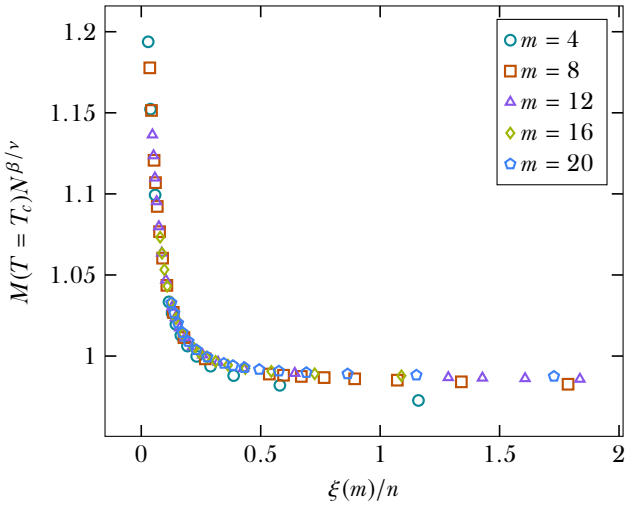

Figure 7.2: Scaling function $\mathcal{G}(\xi(m)/N)$ given in Eq. 7.3.

7.1.2 Central charge

We may directly verify the value of the central charge c associated with the conformal field theory at the critical point by fitting to

$$S_{\text{classical}} \propto \frac{c}{6} \log \xi(m), \tag{7.5}$$

which yields $c = 0.501$, shown in the left panel of Fig. 7.4.

The right panel of Fig. 7.4 shows the fit to the scaling relation in N (or, equivalently the number of CTMRG steps n)

$$S_{\text{classical}} \propto \frac{c}{6} \log N, \tag{7.6}$$

which yields $c = 0.499$.

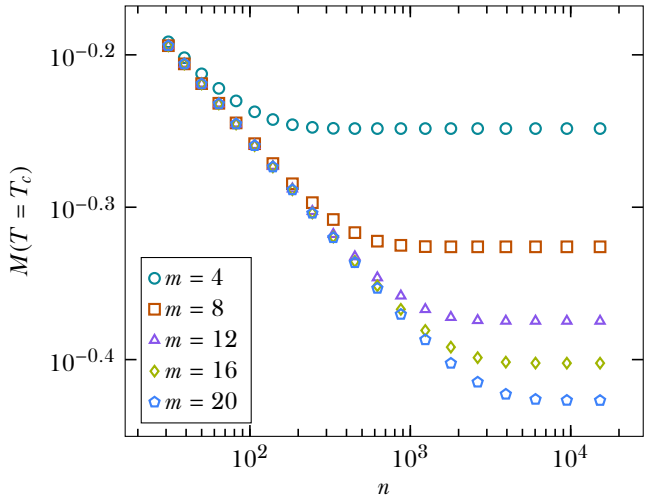

Figure 7.3: Behaviour of the order parameter at fixed m as function of the number of renormalization steps n. For small n, all curves coincide, since the system size is the only limiting length scale. For large enough n, the order parameter is only limited by the length scale $\xi(m)$. In between, there is a cross-over described by $\mathcal{G}(\xi(m)/N)$, given in Eq. 7.3.

7.1.3 Using the entropy to define the correlation length

Via Eq. 5.9, the correlation length is expressed as

$$\xi \propto \exp(\frac{6}{c}S). \tag{7.7}$$

Fig. 7.5 shows the results of fitting the relation in Eq. 7.1 with this definition of the correlation length. The fit is an order of magnitude better in the least-squares sense, and the half-moon shapes have almost disappeared, yielding a much more robust exponent of $\beta/\nu = 0.12498$.

The entropy uses all eigenvalues of the corner transfer matrix, making it apparently less prone to structure in the spectrum than the correlation length as defined in Eq. 5.1, which uses only two eigenvalues of the row-to-row trans-

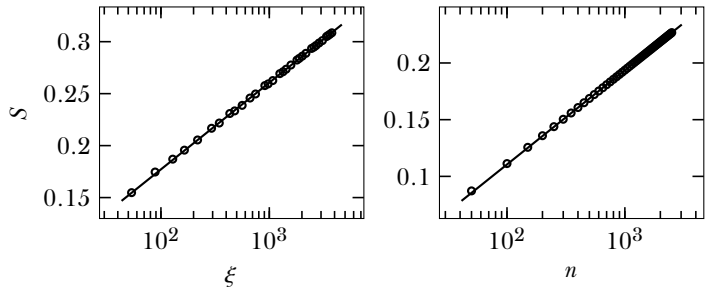

Figure 7.4: Left panel: numerical fit to Eq. 7.5, yielding $c = 0.501$. Here, $m \in \{8, 10, \ldots, 70\}$ and the convergence threshold $\epsilon = 10^{-9}$. Right panel: numerical fit to Eq. 7.6, yielding $c = 0.499$, with the fit made to $n \in \{1500, 1550, \ldots 2500\}$, such that the truncation error is smaller than 10^{-7}.

fer matrix. Furthermore, the corner transfer matrix A is kept diagonal in the CTMRG algorithm, so S is much cheaper to compute than ξ.

7.1.4 Exponent κ

We now check the validity of the relation

$$\xi(m) \propto m^{\kappa} \tag{7.8}$$

in the context of the CTMRG method for two-dimensional classical systems. Similar checks were done for one-dimensional quantum systems in [34].

Let us first state that boundary conditions are relevant. From section 3.7 we expect that for fixed boundary conditions, the entropy and therefore the correlation length is lower for a given bond dimension m.

There are various ways of extracting the exponent κ. Fig. 7.6 shows the results for fixed boundary conditions and Fig. 7.7 for free boundary conditions.

Directly checking Eq. 7.8 yields $\kappa = 1.93$ for a fixed boundary and $\kappa = 1.96$ for a free boundary.

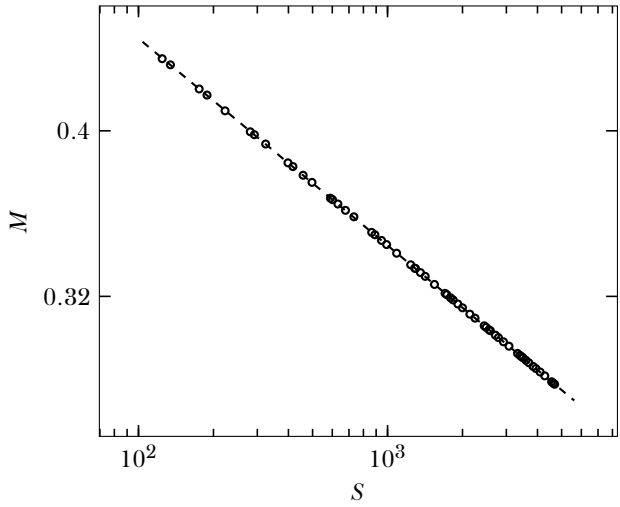

Figure 7.5: Fit to Eq. 7.1, using Eq. 7.7 as the definition of the correlation length. For the fit, we have used $m \in \{10, 11, \ldots, 66\}$, calculated with convergence threshold $\epsilon = 10^{-9}$, yielding $\beta/\nu = 0.12498$.

Under the assumption of Eq. 7.8, we have the following scaling laws at the critical point

$$M(m) \propto m^{-\beta\kappa/\nu} \tag{7.9}$$

$$f(m) - f_{\text{exact}} \propto m^{(2-\alpha)\kappa/\nu} \tag{7.10}$$

for the order parameter and the singular part of the free energy, respectively. With a fixed boundary, a fit to $M(m)$ yields $\kappa = 1.93$. For a free boundary we cannot extract any exponent, since $M = 0$ for every temperature. A fit to $f(m) - f_{\text{exact}}$ yields $\kappa = 1.90$ for a fixed boundary and $\kappa = 1.93$ for a free boundary. Fig. 7.6. Here, we have used $\beta = 1/8$, $\nu = 1$ and $\alpha = 0$ for the Ising model.

We may use Eq. 5.9 and Eq. 3.57 to check the relation

$$S_{\text{classical}} \propto \frac{c\kappa}{6} \log m, \tag{7.11}$$

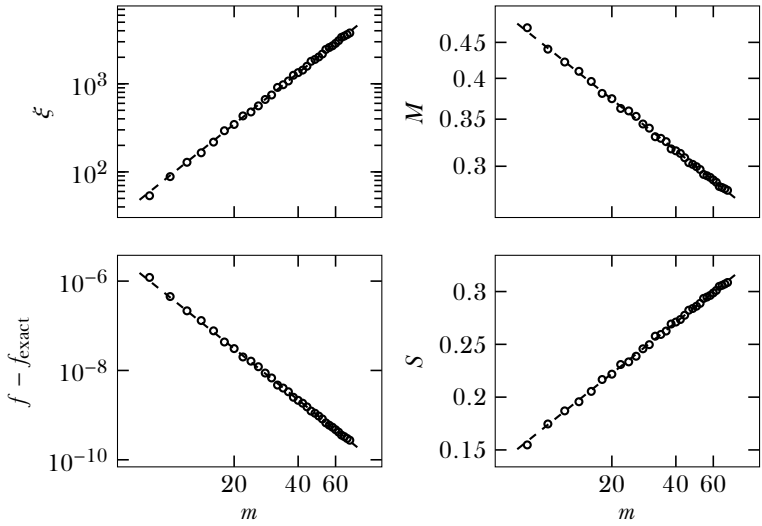

Figure 7.6: Numerical evidence for Eq. 7.8, Eq. 7.9, Eq. 7.11 with fixed boundary, yielding, from left to right and top to bottom, $\kappa = \{1.93, 1.93, 1.90, 1.93\}$. These values have been calculated from simulations with $m \in \{8, 10, \ldots, 70\}$ and convergence threshold $\epsilon = 10^{-9}$.

which yields $\kappa = 1.93$ for a fixed boundary and $\kappa = 1.96$ for a free boundary, with $c = 1/2$ for the Ising model.

7.1.4.1 Comparison with exact result in asymptotic limit

The predicted value for κ [33] is $2.034\ldots$ (see also Eq. 5.22). With the CTMRG method, we extract the slightly lower value of 1.96 (corresponding to free boundary conditions). But, the structure in the quantities as function of m makes it hard to get an accurate fit to κ.

It is interesting to note that for fixed boundary conditions, the relation in Eq. 7.8 holds, but with a lower exponent κ. This is to be expected, since half the spectrum of the corner transfer matrix is missing.

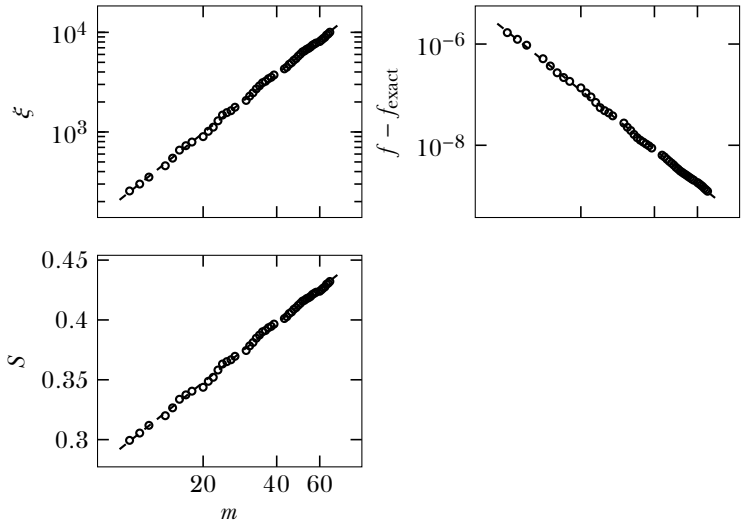

Figure 7.7: Numerical evidence for Eq. 7.8 with free boundary, yielding from left to right and then bottom $\kappa = \{1.96, 1.93, 1.96\}$. These values have been calculated from simulations with $m \in \{10, 11, \ldots, 66\}$, but with $m \in \{13, 19, 28, 29, 40, 41, 42, 59\}$ left out, because for those values m the system breaks its symmetry (see section 3.7.2). The convergence threshold was chosen to be $\epsilon = 10^{-7}$. It is not lower since more values m break symmetry as machine precision is approached.

7.2 Locating the critical point

In general, the critical point is not known, but it may be located using the spectrum of the corner transfer matrix as described in section 5.4. For a given value of m (or N, in a finite-size approximation), the pseudocritical temperature is defined as the point of maximum entropy.

Fig. 7.8 shows the classical analogue to the entanglement entropy as a function of temperature for different values of m.

The critical point is located by fitting the scaling law in Eq. 4.6.

7.2.1 Finite m

For approximations with finite bond dimension m, it is not clear what length scale should be used to fit the scaling behaviour of $T^\star(m)$. Fig. 7.9 shows the fits for different choices of this length scale. The results are tabulated in Table 7.1. To obtain $T^\star$, we have calculated $T^\star(m)$ for $m \in \{10, 11, \ldots, 60\}$ with a convergence threshold of 10^{-8} and a temperature tolerance of 10^{-8}. The boundaries are fixed to +1.

We denote the estimated value of the critical temperature as $\widetilde{T_c}$. Recall that the exact value is

$$T_c = 2.2691853\ldots \tag{7.12}$$

and

$$\nu = 1. \tag{7.13}$$

When using $\xi(T_c, m)$, the correlation length at the exact critical point, the result shows a lot of structure, yielding $\widetilde{T_c} = 2.269172$ and $\nu = 1.057$.

If, instead, the correlation length at the estimated pseudocritical temperature $\xi(T^\star(m))$ is used, the data shows less structure and we obtain the much more precise results $\widetilde{T_c} = 2.269183$ and $\nu = 1.002$.

Another option is to use the entropy to define the correlation length, via Eq. 7.7, which gave more accurate results than using the transfer matrix definition in section 7.1.3. In this case, the results are slightly worse than the transfer matrix definition: $T_c = 2.269183$ and $\nu = 1.02$.

Finally, we may directly fit the law

$$|T_c - T^\star(m)| \propto m^{-\kappa/\nu}, \tag{7.14}$$

yielding $T_c = 2.269181$ and $\kappa/\nu = 1.91$. Incidentally, this is another way to confirm $\kappa \approx 1.9$ for systems with a fixed boundary.

Why do length scales defined at $T^\star$ work better?? It is fortunate that we don't need the length scales at T_c, since we don't know it.

7.2.2 Finite N

As a cross check, we can instead use systems of finite size to extract T_c and ν. We have calculated $T^\star(n)$ for $n \in \{2300, 2500, \ldots, 7900\}$, with m big enough such that the truncation error is no larger than 10^{-6}. This yields $T_c = 2.269185$ and $\nu = 0.98$.

N_{eff}	T_c	ν
$\xi(T_c, m)$	2.269172	1.057
$\xi(T^\star(m))$	2.269183	1.002
$\exp((6/c)S(T^\star(m))$	2.269183	1.02
m^κ	2.269181	–
N	2.269185	0.98

Table 7.1: Results for fits to the scaling law Eq. 4.6 using different length scales. When using m^κ, $\kappa \approx 1.91$ was found to give the best fit.

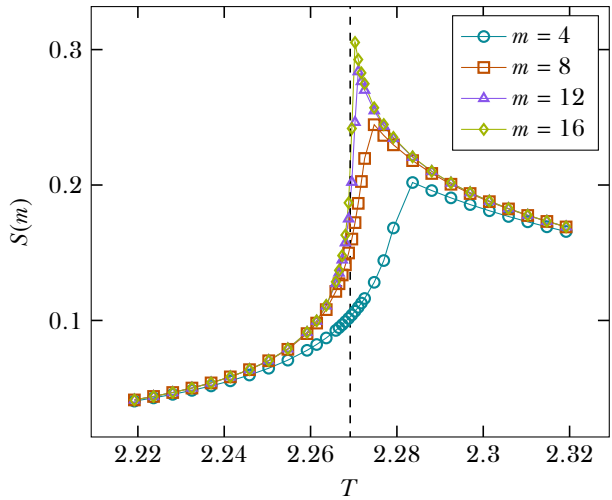

Figure 7.8: Classical analogue to the entanglement entropy, as in Eq. 3.57, near the critical point (shown as dashed line).

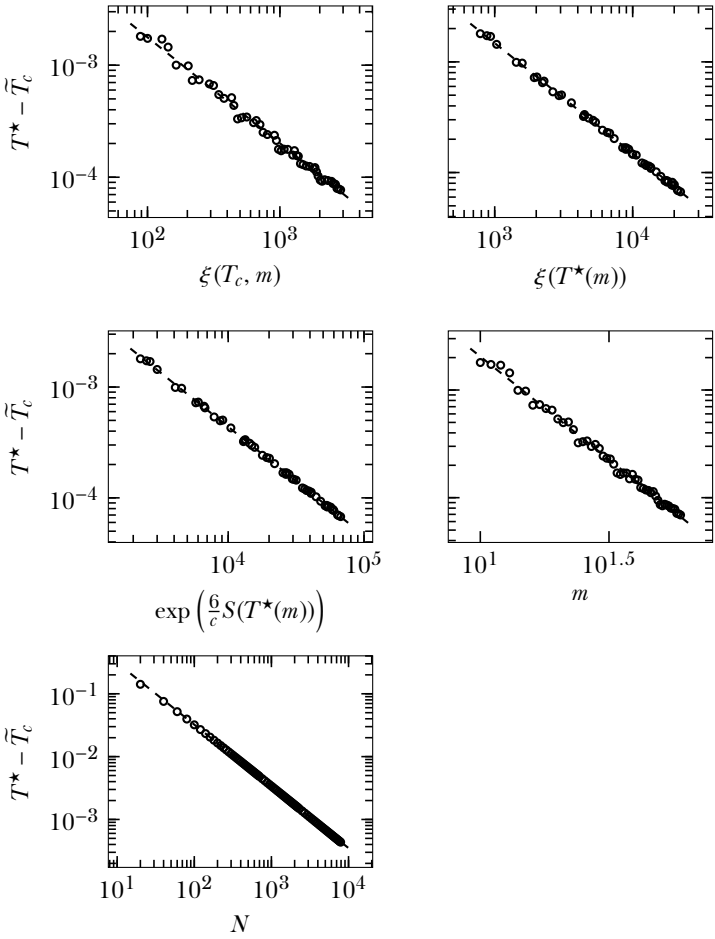

Figure 7.9: Fits to the scaling law Eq. 4.6. Results for the critical temperature and exponent ν are tabulated in Table 7.1.

N_{eff}	fitness P
$\xi(T_c, m)$	0.0075
$\xi(T^\star(m))$	0.066
$\exp((6/c)S(T_c, m))$	0.057
$\exp((6/c)S(T^\star(m))$	0.087
m^κ	0.0080
N	0.0075

Table 7.2: Fitness of data collapse (Eq. 4.23) for different length scales. $\kappa \approx 1.98$ was found to be optimal for the length scale m^κ.

7.3 Away from the critical point

We may also verify the validity of the different length scales by asserting that the data for different values of m should collapse on a single curve

$$\mathcal{G}(tN_{\text{eff}}(m)^{1/\nu}) = M(T, m)N_{\text{eff}}(m)^{\beta/\nu}. \tag{7.15}$$

All data points were calculated with a convergence threshold of 10^{-7}. The values of the pseudocritical temperatures are taken from the results in section 7.2. No temperatures beyond T_c is considered because the order parameter drops off sharply, causing the curve $\mathcal{G}(x)$ to tend to zero almost vertically, making the fitness P unreliable.

Fig. 7.10 shows that for all length scales, the results more or less fall on one curve. Table 7.2 shows the fitness of the data collapse [28] (given by Eq. 4.23) for all length scales used.

Say which length scales apparently don't work so well

Using m^κ as a length scale for optimized fitness $P(\kappa)$ yields $\kappa \approx 1.98$, substantially higher than found previously for fixed boundary conditions.

As a cross-check, the bottom-right panel of Fig. 7.10 shows data points for finite-N simulations. Here, the bond dimension is chosen such that the truncation error is smaller than 10^{-6}.

7.4 Conclusions

TODO

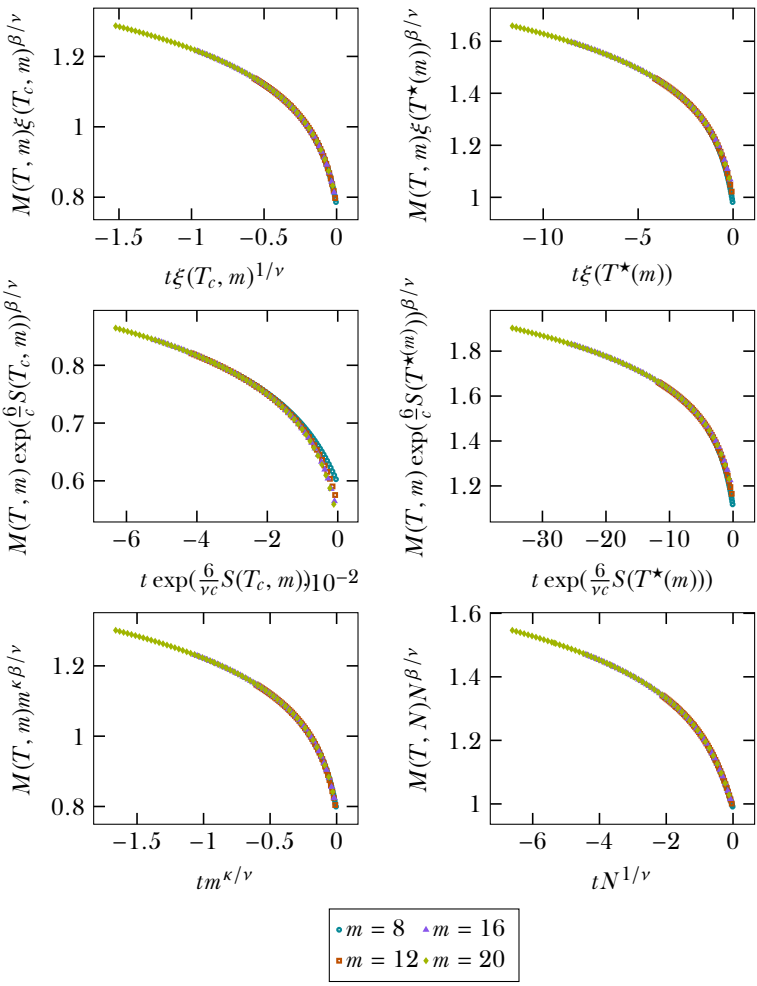

Figure 7.10: Data collapses using different length scales. For the bottom-right plot, approximations with finite N instead of finite m have been used, with $n = \{160, 480, 1000, 1500\}$ ($n = \frac{N-1}{2}$ is the number of algorithm steps).

8
Numerical results for the clock model

We present results of scaling in bond dimension and system size with the CTMRG algorithm for the five- and six-state clock model.

Not finished yet.

8.1 Introduction

In the field of phase transitions and critical phenomena, the two-dimensional topological phase transition discovered by Kosterlitz and Thouless [50, 51] received much attention. This phase transition is characterized not by an order parameter which indicates a breaking of symmetry, but by the proliferation of topological defects.

In the low-temperature phase, the two-point correlation functions decay with a power-law with varying exponent $\eta(T)$. At the transition, the correlation length diverges as

$$\xi \propto \exp(A|T - T_c|^{-1/2}), \tag{8.1}$$

with A a non-universal constant. Above the transition, the two-point correlators decay exponentially.

The XY model consists of planar rotors on the square lattice. It exhibits the Kosterlitz-Thouless (BK) phase transition and by the Mermin-Wagner-Hohenberg theorem the symmetry of the ground state is broken for all temperatures, due to the $O(2)$ (planar rotational) symmetry of the potential [52, 53].

The q-state clock model possesses the discrete $\mathbb{Z}_q$ symmetry and is an interpolation between the Ising model, which corresponds to $q = 2$, and the XY

model, which corresponds to $q \to \infty$. Its energy function is given by

$$H_q = -\sum_{\langle ij \rangle} \cos(\theta_i - \theta_j), \tag{8.2}$$

with the spins taking the values

$$\theta = \frac{2\pi n}{q} \qquad n \in \{0, \ldots, q-1\}. \tag{8.3}$$

It has been proven that for high enough q, this model indeed exhibits a Kosterlitz-Thouless transition [54]. Furthermore, it has been proven that for $q \geq 5$, a general model with $\mathbb{Z}_q$ symmetry (of which Eq. 8.2 is a special case) has three phases: a symmetry broken phase for $T < T_1$, an intermediate phase with power law decay of the correlation function, and a high-temperature phase with exponential decay of the correlation function for $T > T_2$ [55].

In the Villain formulation of the potential [56], it has been proven that the transition at T_2 is a BK-transition [57], and numerical results suggest that for a broad range of temperatures, the thermodynamic behaviour becomes identical to the XY model for high enough q [58].

For the model in Eq. 8.2, the phase diagram and the value q_c for which it first exhibits a BK-transition are not precisely known, making it a good candidate for numerical investigation. We briefly summarise previous numerical results below.

8.2 Previous numerical results

- [59] 2014 claims BK-transition for $q = 5$ by discrete helicity modulus using TMRG.
- [60] 2013 claims BK-transition for $q = 5$ by discrete helicity modelus using Monte Carlo. Shows infinitesimal helicity modulus does not vanish for finite q.
- [61] 2011 most comprehensive study? Claims BK-transition for $q = 5$ by calculating Binder cumulants + stuff I don't understand using Monte Carlo.
- [62] 2012 don't understand. Some numerical and theoretical validations for certain assumptions for high q.

- [63] 2010 claims that $q = 5$ exhibits non-KT-transition, based on the fact that their (wrong) definition of the helicity modulus does not vanish.
- [64] 2013 claims that $q = 5$ exhibits weaker cousin of KT-transition, based on things I do not fully understand, but among others on the correct, discrete definition of the helicity modulus (true?).
- [65] 2017 uses partition function zeros (don't understand that concept) to show that the behaviour of zeros of the $q = 5$ model significantly departs from the behaviour of $q \geq 6$.

8.3 Results

What are the results that really should be in there? Focus on $q = 5, 6$.

- show that scaling relation holds for magnetization and correlation length and calculate exponent. Should vary as $\eta \propto T$ in the massless phase and probably (?) $\eta(T_2) = 1/4$ and $\eta(T_1) \propto 1/q^2$ or something.
- show that $c = 1$ massless phase exists.
- show that $T^\star - T_c$ is compatible with correlation length at essential singularity (but what about logarithmic corrections...?)
- data collapse in magnetization around Kosterlitz-transition

A

Correspondence of quantum and classical lattice systems

The partition of a discrete quantum mechanical system is given by

$$Z_q = \operatorname{Tr} \exp(-\beta H_q) = \sum_{\sigma} \langle \sigma | \exp(-\beta H_q) | \sigma \rangle \tag{A.1}$$

Imagine splitting the imaginary time interval β into N smaller steps:

$$\beta = N \delta\tau, \tag{A.2}$$

$$\exp(-\beta H_q) = \exp(-\delta\tau H_q)^N . \tag{A.3}$$

Recall that for any orthonormal basis, the identity can be expressed as a sum over projectors onto the basis states

$$\mathbb{1} = \sum_{\sigma} |\sigma\rangle \langle \sigma| . \tag{A.4}$$

If we insert $N - 1$ resolutions of indentity into Eq. A.1, we obtain

$$Z_q = \sum_{\sigma} \sum_{\sigma_1, \ldots, \sigma_{N-1}} \langle \sigma | \exp(-\beta \delta\tau) | \sigma_1 \rangle \ldots \langle \sigma_{N-1} | \exp(-\beta \delta\tau) | \sigma \rangle . \tag{A.5}$$

This is the imaginary time path integral formulation of quantum mechanics. Similar to the real-time path integral, an evolution in the imaginary time direction is expressed as a sum over all paths connecting the initial and final state, which are the same here, since we are taking the trace.

We turn to the partition function of a classical system, written as a product of its transfer matrix, as in Eq. 3.11:

$$Z_{\mathrm{cl}} = \operatorname{Tr} T^N . \tag{A.6}$$

There is a striking similarity between a quantum mechanical partition function in d dimensions and a classical partition function in $d + 1$ dimensions. Adding a row to the classical lattice by applying the transfer matrix corresponds to time evolution of a quantum system:

$$T \longleftrightarrow \exp(-\delta\tau H_q). \tag{A.7}$$

The classical temperature corresponds to the coupling constants in the Hamiltonian H_q.

Letting $\beta \to \infty$ (or equivalently $T \to 0$) amounts to taking $N \to \infty$, while keeping $\delta\tau$ fixed. In this limit, analogously to the transfer matrix for the classical system (cf. Eq. 3.19), the operator $\exp(-\beta H_\mathrm{q})$ becomes a projector onto the ground state.

Thus, a quantum lattice in the ground state corresponds to a classical lattice that is infinite in its additional dimension.

What is the role $\delta\tau$? Why should it be small? If we want to make the correspondence $T \equiv H_q$, we need $\delta\tau \to 0$. But what does this imply for the lattice? How does the 'scaling limit' come into play? Also: explain the correspondence between the energy scale of the quantum system and the correlation length of the classical system. Maybe do an example of 0D quantum to 1D classical and 1D quantum to 2D classical (Ising model?).

B
Introduction to tensor networks

B.1 Tensors, or multidimensional arrays

In the field of tensor networks, a tensor is a multidimensional table with numbers – a convenient way to organize information. It is the generalization of a vector

$$v_i = \begin{bmatrix} v_1 \\ \vdots \\ v_n \end{bmatrix}, \tag{B.1}$$

which has one index, and a matrix

$$M_{ij} = \begin{bmatrix} M_{11} & \dots & M_{1n} \\ \vdots & & \vdots \\ M_{m1} & \dots & M_{mn} \end{bmatrix}, \tag{B.2}$$

which has two. A tensor of rank N has N indices:[1]

$$T_{i_1 \dots i_N}. \tag{B.3}$$

A tensor of rank zero is just a scalar.

[1] The definition of rank in this context is not to be confused with the rank of a matrix, which is the number of linearly independent columns. Synonyms of tensor rank are tensor degree and tensor order.

B.2 Tensor contraction

Tensor contraction is the higher-dimensional generalization of the dot product

$$\boldsymbol{a} \cdot \boldsymbol{b} = \sum_i a_i b_i, \tag{B.4}$$

where a lower-dimensional tensor (in this case, a scalar, which is a zero-dimensional tensor) is obtained by summing over all values of a repeated index.

Examples are matrix-vector multiplication

$$(M\boldsymbol{a})_i = \sum_j M_{ij} a_j, \tag{B.5}$$

and matrix-matrix multiplication

$$(AB)_{ij} = \sum_k A_{ik} B_{kj}, \tag{B.6}$$

but a more elaborate tensor multiplication could look like

$$w_{abc} = \sum_{d,e,f} T_{abcdef} v_{def}. \tag{B.7}$$

As with the dot product between vectors, matrix-vector multiplication and matrix-matrix multiplication, a contraction between tensors is only defined if the dimensions of the indices match.

B.3 Tensor networks

A tensor network is specified by a set of tensors, together with a set of contractions to be performed. For example:

$$M_{ab} = \sum_{i,j,k} A_{ai} B_{ij} C_{jk} D_{kb}, \tag{B.8}$$

which corresponds to the matrix product $ABCD$.

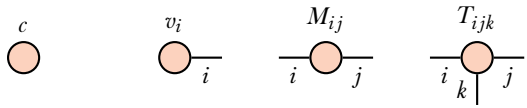

Figure B.1: Open-ended lines, called legs, represent unsummed indices. A tensor with no open legs is a scalar.

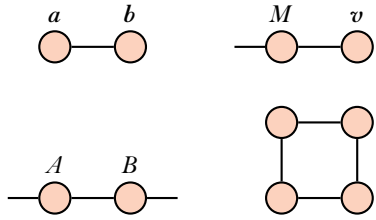

Figure B.2: Connected legs represent contracted indices. The networks in the figure represent $\sum_i a_i b_i$ (dot product), $\sum_j M_{ij} a_j$ (matrix-vector product), $\sum_k A_{ik} B_{kj}$ (matrix-matrix product) and $\mathrm{Tr}\, ABCD$, respectively.

B.3.1 Graphical notation

It is highly convenient to introduce a graphical notation that is common in the tensor network community. It greatly simplifies expressions and makes certain properties manifest.

Each tensor is represented by a shape. Open-ended lines, called legs, represent unsummed indices. See Fig. B.1. If it clear from the context, index labels may be omitted from the open legs.

Each contracted index is represented by a connected line. See Fig. B.2.

Many tensor equations, while burdensome when written out, are readily understood in this graphical way. As an example, consider the matrix trace in Fig. B.2, where its cyclic property is manifest.

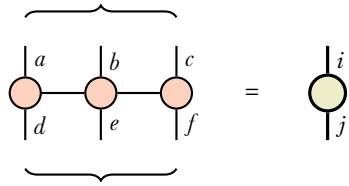

Figure B.3: Reshaping a tensor T_{abcdef} to T_{ij}

B.3.2 Reshaping tensors

Several indices can be taken together to form a single, joint index, that runs over all combinations of the indices that fused into it. For example, an $m \times n$ matrix can be reshaped into an mn vector.

$$M_{ij} = v_a \qquad a \in \{1, \ldots, mn\}. \tag{B.9}$$

Some convention has to be chosen to map the joint index i, j onto the single index a, for example

$$a = (n-1)i + j, \tag{B.10}$$

which orders the indices of the matrix M row by row

$$11, 12, \ldots, 1n, 21, 22, \ldots, mn-1, mn. \tag{B.11}$$

Graphically, an index contraction is represented as a bundling of the open legs of a tensor network. See Fig. B.3 for an example.

B.3.3 Computational complexity of contraction

Computational complexity.

Bibliography

[1] S. R. White, "Density matrix formulation for quantum renormalization groups", Physical Review Letters **69**, 2863 (1992).

[2] K. G. Wilson, "The renormalization group: critical phenomena and the Kondo problem", Reviews of Modern Physics **47**, 773 (1975).

[3] D. Poulin, A. Qarry, R. Somma, and F. Verstraete, "Quantum simulation of time-dependent Hamiltonians and the convenient illusion of Hilbert space", Physical Review Letters **106**, 170501 (2011).

[4] S. R. White, and R. M. Noack, "Real-space quantum renormalization groups", Physical Review Letters **68**, 3487 (1992).

[5] R. M. Noack, and S. R. White, "The density matrix renormalization group", in *Density-matrix renormalization, a new numerical method in physics*, Vol. 528, edited by I. Peschel, X. Want, M. Kaulke, and K. Hallberg, (1999) Chap. 2.

[6] U. Schollwöck, "The density-matrix renormalization group", Reviews of modern physics **77**, 263–265 (2005).

[7] S. R. White, "Density-matrix algorithms for quantum renormalization groups", Physical Review B **48**, 10345 (1993).

[8] R. B. Lehoucq, and D. C. Sorensen, "Deflation techniques for an implicitly restarted Arnoldi iteration", SIAM Journal on Matrix Analysis and Applications **17**, 789–821 (1996).

[9] T. Nishino, "Density matrix renormalization group method for 2D classical models", Journal of the Physical Society of Japan **64**, 3598–3601 (1995).

[10] T. Nishino, and K. Okunishi, "Corner transfer matrix renormalization group method", Journal of the Physical Society of Japan **65**, 891–894 (1996).

[11] R. J. Baxter, "Dimers on a rectangular lattice", Journal of Mathematical Physics **9**, 650–654 (1968).

[12] R. J. Baxter, "Variational approximations for square lattice models in statistical mechanics", Journal of Statistical Physics **19**, 461–478 (1978).

[13] R. J. Baxter, *Exactly solved models in statistical mechanics* (Elsevier, 1982) Chap. 13.

[14] D. Tong, *Lectures on statistical physics*, (2011) http://www.damtp.cam.ac.uk/user/tong/statphys.html (visited on 06/07/2017).

[15] E. Ising, "Beitrag zur theorie des ferromagnetismus", Zeitschrift für Physik **31**, 253–258 (1925).

[16] T. Nishino, and K. Okunishi, "Corner transfer matrix algorithm for classical renormalization group", Journal of the Physical Society of Japan **66**, 3040–3047 (1997).

[17] C.-Y. Huang, T.-C. Wei, and R. Orús, "Holographic encoding of universality in corner spectra", Physical Review B **95**, 195170 (2017).

[18] R. Orús, "Exploring corner transfer matrices and corner tensors for the classical simulation of quantum lattice systems", Physical Review B **85**, 205117 (2012).

[19] I. Peschel, and V. Eisler, "Reduced density matrices and entanglement entropy in free lattice models", Journal of Physics A: Mathematical and Theoretical **42**, 504003 (2009).

[20] I. Peschel, M. Kaulke, and Ö. Legeza, "Density-matrix spectra for integrable models", Annalen der Physik **8**, 153–164 (1999).

[21] B. Davies, "Corner transfer matrices for the Ising model", Physica A: Statistical Mechanics and its Applications **154**, 1–20 (1988).

[22] K. Okunishi, Y. Hieida, and Y. Akutsu, "Universal asymptotic eigenvalue distribution of density matrices and corner transfer matrices in the thermodynamic limit", Physical Review E **59**, R6227 (1999).

[23] M. N. Barber, "Finite-size scaling", in *Phase transitions and critical phenomena*, Vol. 8, edited by C. Domb, and J. L. Lebowitz, (Academic press, 1983) Chap. 2.

[24] L. P. Kadanoff, "More is the same; phase transitions and mean field theories", Journal of Statistical Physics **137**, 777 (2009).

[25] G. Jaeger, "The Ehrenfest classification of phase transitions: introduction and evolution", Archive for history of exact sciences **53**, 51–81 (1998).

[26] M. E. Fisher, and A. E. Ferdinand, "Interfacial, boundary, and size effects at critical points", Physical Review Letters **19**, 169 (1967).

[27] M. E. Fisher, and M. N. Barber, "Scaling theory for finite-size effects in the critical region", Physical Review Letters **28**, 1516 (1972).

[28] S. M. Bhattacharjee, and F. Seno, "A measure of data collapse for scaling", Journal of Physics A: Mathematical and General **34**, 6375 (2001).

[29] T. Nishino, K. Okunishi, and M. Kikuchi, "Numerical renormalization group at criticality", Physics Letters A **213**, 69–72 (1996).

[30] S. Östlund, and S. Rommer, "Thermodynamic limit of density matrix renormalization", Physical Review Letters **75**, 3537 (1995).

[31] M. M. Wolf, G. Ortiz, F. Verstraete, and J. I. Cirac, "Quantum phase transitions in matrix product systems", Physical Review Letters **97**, 110403 (2006).

[32] S. Rommer, and S. Östlund, "Class of ansatz wave functions for one-dimensional spin systems and their relation to the density matrix renormalization group", Physical Review B **55**, 2164 (1997).

[33] F. Pollmann, S. Mukerjee, A. M. Turner, and J. E. Moore, "Theory of finite-entanglement scaling at one-dimensional quantum critical points", Physical Review Letters **102**, 255701 (2009).

[34] L. Tagliacozzo, T. R. De Oliveira, S. Iblisdir, and J. I. Latorre, "Scaling of entanglement support for matrix product states", Physical Review B **78**, 024410 (2008).

[35] M. Andersson, M. Boman, and S. Östlund, "Density-matrix renormalization group for a gapless system of free fermions", Physical Review B **59**, 10493 (1999).

[36] R. J. Baxter, *Exactly solved models in statistical mechanics* (Elsevier, 1982) Chap. 7.

[37] G. Vidal, "Classical simulation of infinite-size quantum lattice systems in one spatial dimension", Physical Review Letters **98**, 070201 (2007).

[38] P. Calabrese, and J. Cardy, "Entanglement entropy and quantum field theory", Journal of Statistical Mechanics: Theory and Experiment **2004**, P06002 (2004).

[39] G. Vidal, J. I. Latorre, E. Rico, and A. Kitaev, "Entanglement in quantum critical phenomena", Physical Review Letters **90**, 227902 (2003).

[40] E. Ercolessi, S. Evangelisti, and F. Ravanini, "Exact entanglement entropy of the XYZ model and its sine-Gordon limit", Physics Letters A **374**, 2101–2105 (2010).

[41] I. Affleck, "Universal term in the free energy at a critical point and the conformal anomaly", Physical Review Letters **56**, 746 (1986).

[42] E. Lieb, T. Schultz, and D. Mattis, "Two soluble models of an antiferromagnetic chain", Annals of Physics **16**, 407–466 (1961).

[43] G. J. Mata, and G. B. Arnold, "Energy gap, dynamic correlations, and correlation length in two-dimensional antiferromagnets", Physical Review B **39**, 9768 (1989).

[44] P. Pfeuty, "The one-dimensional Ising model with a transverse field", Annals of Physics **57**, 79–90 (1970).

[45] P. Calabrese, and A. Lefevre, "Entanglement spectrum in one-dimensional systems", Physical Review A **78**, 032329 (2008).

[46] T. J. Osborne, and M. A. Nielsen, "Entanglement in a simple quantum phase transition", Physical Review A **66**, 032110 (2002).

[47] R. Krčmár, and L. Šamaj, "Reentrant disorder-disorder transitions in generalized multicomponent Widom-Rowlinson models", Physical Review E **92**, 052103 (2015).

[48] R. Krcmar, A. Gendiar, and T. Nishino, "Phase diagram of a truncated tetrahedral model", Physical Review E **94**, 022134 (2016).

[49] R. Krčmár, A. Gendiar, and T. Nishino, "Phase transition of the six-state clock model observed from the entanglement entropy", arXiv:1612.07611 (2016).

[50] J. M. Kosterlitz, and D. J. Thouless, "Ordering, metastability and phase transitions in two-dimensional systems", Journal of Physics C: Solid State Physics **6**, 1181 (1973).

[51] J. M. Kosterlitz, "The critical properties of the two-dimensional xy model", Journal of Physics C: Solid State Physics **7**, 1046 (1974).

[52] N. D. Mermin, and H. Wagner, "Absence of ferromagnetism or antiferromagnetism in one-or two-dimensional isotropic Heisenberg models", Physical Review Letters **17**, 1133 (1966).

[53] P. C. Hohenberg, "Existence of long-range order in one and two dimensions", Physical Review **158**, 383 (1967).

[54] J. Fröhlich, and T. Spencer, "The Kosterlitz-Thouless transition in two-dimensional abelian spin systems and the Coulomb gas", Communications in Mathematical Physics **81**, 527–602 (1981).

[55] J. Cardy, "General discrete planar models in two dimensions: duality properties and phase diagrams", Journal of Physics A: Mathematical and General **13**, 1507 (1980).

[56] J. Villain, "Theory of one-and two-dimensional magnets with an easy magnetization plane. II. the planar, classical, two-dimensional magnet", Journal de Physique **36**, 581–590 (1975).

[57] J. V. José, L. P. Kadanoff, S. Kirkpatrick, and D. R. Nelson, "Renormalization, vortices, and symmetry-breaking perturbations in the two-dimensional planar model", Physical Review B **16**, 1217 (1977).

[58] C. M. Lapilli, P. Pfeifer, and C. Wexler, "Universality away from critical points in two-dimensional phase transitions", Physical Review Letters **96**, 140603 (2006).

[59] C. Chatelain, "DMRG study of the Berezinskii–Kosterlitz–Thouless transitions of the 2D five-state clock model", Journal of Statistical Mechanics: Theory and Experiment **2014**, P11022 (2014).

[60] Y. Kumano, K. Hukushima, Y. Tomita, and M. Oshikawa, "Response to a twist in systems with Z_p symmetry: the two-dimensional p-state clock model", Physical Review B **88**, 104427 (2013).

[61] O. Borisenko, G. Cortese, R. Fiore, M. Gravina, and A. Papa, "Numerical study of the phase transitions in the two-dimensional $Z(5)$ vector model", Physical Review E **83**, 041120 (2011).

[62] O. Borisenko, V. Chelnokov, G. Cortese, R. Fiore, M. Gravina, and A. Papa, "Phase transitions in two-dimensional $Z(N)$ vector models for $N > 4$", Physical Review E **85**, 021114 (2012).

[63] S. K. Baek, and P. Minnhagen, "Non-Kosterlitz-Thouless transitions for the q-state clock models", Physical Review E **82**, 031102 (2010).

[64] S. K. Baek, H. Mäkelä, P. Minnhagen, and B. J. Kim, "Residual discrete symmetry of the five-state clock model", Physical Review E **88**, 012125 (2013).

[65] D.-H. Kim, "Partition function zeros of the p-state clock model in the complex temperature plane", arXiv:1704.04973 (2017).